Stony Brook University

Rapid Laser Scanning Based Surface Texturing for Energy Applications

A Thesis Presented

by

Matthew Quigley

to

The Graduate School

in Partial Fulfillment of the

Requirements

for the Degree of

Master of Science

in

Mechanical Engineering

Stony Brook University

May 2012

Stony Brook University

The Graduate School

Matthew Quigley

We, the thesis committee for the above candidate for the

Master of Science degree, hereby recommend

acceptance of this thesis.

Dr. David Hwang – Thesis Advisor
Assistant Professor, Mechanical Engineering

Dr. Jon Longtin – Second Reader
Associate Professor, Mechanical Engineering

Dr. John Kincaid – Third Reader
Professor, Mechanical Engineering

This thesis is accepted by the Graduate School

Charles Taber
Interim Dean of the Graduate School

Abstract of the Thesis

Rapid Laser Scanning Based Surface Texturing for Energy Applications

by

Matthew Quigley

Master of Science

in

Mechanical Engineering

Stony Brook University

2012

Extensive research in micro/nano scale surface engineering has developed a variety of energy applications, including the improvement of light trapping in solar cells. The motivation for this work is the issues that come with nonrenewable energy, the dominating source of energy in this country. Renewable energy is clean and quiet. In particular, solar energy can generate enough power on its own to sustain the country. The current issue with this technology is its high manufacturing costs and low efficiencies.

A solution to these challenges is through laser induced surface texturing. Laser induced surface texturing is an effective tool to roughen the surface of silicon, minimizing reflection and subsequently enhancing absorption through the creation of spiked structures. Extensive research has been conducted in this field already. So-called black silicon has been created and demonstrates enhanced absorption characteristics. However, the black silicon created is not yet ideal. In some cases, spikes are created on the microscale, but the structure is not spatially uniform, which causes problems for adaptation to manufacturing processes. In other cases, uniformity is attained, but high ablation causes loose structures to be formed, leading to a decrease in current density, which is equivalent to a reduction in solar cell performance. In all cases, additional chemical etching steps are required in order to get the desired results.

The focus of this thesis is on creating black silicon by coupling a raster scan from a X-Y scanning system with a nanosecond laser with a Gaussian beam profile. An arbitrary sized area can be processed uniformly. Secondary heating allows for annealing of the previously created spikes, increasing homogeneity and current density of the overall solar cell performance. This would eliminate the needs for additional steps to the manufacturing process. A parametric study was performed by varying: laser power, line spacing, scanning speed, and pulse frequency. The parametric study showed that there was a broad processing range for creating black silicon. The demonstrated results showed great promise for processing of arbitrary sample size and practical processing speeds.

In addition, surface texturing is applicable to broader energy applications. A significant enhancement of emissivity was demonstrated by texturing the surfaces of silicon and copper in uniform and controllable fashion. Texturing these materials can lead to efficiency improvement of solar collectors and heat exchangers.

Laser induced surface texture can be applied to energy application where it is desirable to increase the surface area. Increased surface area on the electrodes of batteries or fuel cells can improve the efficiency and lifetime of these devices. Preliminary results operated at ablation dominated regime showed in fact a decrease in performance, displaying the importance of optimal annealing of the structure. Another use of an increased surface area is a boost of algae growth for massive bio-fuel production. An increased surface area can also be used for adhesion/cohesion enhancement of thermal-sprayed thin film for thermo-electrical devices.

In summary, rapid laser scanning based surface texturing results have been demonstrated. The samples created display superior process uniformity at arbitrary sample areas with simultaneous annealing for improved crystallinity. While this process was designed for solar cells, it has great potential for various other energy applications.

TABLE OF CONTENTS

LIST OF FIGURES

LIST OF TABLES

.

ACKNOWLEDGEMENTS

I would like to dedicate this thesis to my family for their continual support.

I would like to thank my advisor, Dr. Hwang, for all of the help he has given me over the past year.

I would like to thank Dr. Longtin for being on my committee, laser lab facility usage in the early stages of this project and valuable discussions. I would like to thank Dr. Kincaid for being on my committee, for reflection measurement, for the IR camera and for exploring energy technology applications.

I would like to thank Di Liu for SEM analysis as well as help with experimental setup. And I would also like to thank Mahder Tewolde for experimental support. I would like to thank Mika Lai and Hallie Golden for their help with checking this thesis for grammar. Additional thanks to the members of the laser solar PV lab.

I would like to thank Stony Brook University and The Advanced Energy Research and Technology Center for funding and lab space. I would like to thank Brookhaven National Labs for use of the scanning electron microscope. I would like to thank Yuco Optics for the donated Nd:YAG nanosecond laser.

CHAPTER 1: INTRODUCTION

Currently, silicon solar cells dominate the commercial industry due to the relatively high abundance of silicon and the relatively low cost compared to other solar cell materials. However, due to their high manufacturing costs, solar cells are still unable to compete with traditional forms of energy (fossil fuels) in cost as well as efficiency. Extensive research is being conducted in this field in order to improve the capabilities of this technology.

Traditional manufacturing processes include cutting silicon wafers from ingots. The surfaces of these wafers have loose structures that degrade the performance of the solar cell. Typical convention is to wet etch the surface of the wafers with KOH to remove the loose structures.

Silicon has a highly reflective surface which reflects a large amount of light. Antireflection coatings are used to decrease reflection, subsequently improving absorption[1]. Antireflection coatings can be applied in a single layer or multi-layer transparent films. Single layer films rely on interference between incident and reflected waves and are designed for particular angles and wavelengths[2]. On the other hand, the multiple layer films reduce reflection by gradually changing the refractive index from air to silicon and thus can reduce the reflection for a broader range of angles and wavelengths.

An alternative to chemical etching and antireflection coatings is surface texturing from pulsed lasers. Surface texturing enhances light trapping through geometric optics. Light that is initially reflected still has a chance to be absorbed, which increases the optical path length of a photon.[3] The optical path length is the distance a photon can travel before it is reflected away from the surface. Thus, surface texturing is able to improve the absorption characteristics of a material.

Surface texturing changes the morphology of the surface, inducing a change in the color by altering the wavelengths that get reflected from the material. Highly absorbing silicon has been dubbed the name black silicon. Research by various organizations and institutions has provided a basis for advancements in this field.

Black silicon can be created by irradiation from femtosecond lasers. It can be formed through purely ablative processes.[4,5] Here, microgrooves are created by ablation to enhance light trapping.

However, no evidence was provided on the effect of ultrafast pulses on the overall carrier diffusion length. It is expected to decrease the overall performance due to loose structures being formed by the ablation, as well as a decrease in the crystallinity of the surface structure.

Another way of created black silicon with femtosecond lasers is to shine a laser on a single spot for a large number pulses[6]. This process creates spiked structures.

The spiked structure grows from the center outward and traps light due to geometric light trapping. Similar to the microgrooves, this process also shows the loose structures from ablation. There are two additional issues: This process requires an environment with an etchant instead of being processed in air. The second issue is that the surface is not uniform, which provides limitations to the size of structures that can be processed at any given time. Black silicon has also been created by pulsing a surface with nanosecond lasers in a vacuum chamber.[7] This result was similar to the femtosecond laser case. The structured surface was not uniform and a chemical etchant was required to remove the defects form the laser processing.

This work focuses on rapid scanning laser processing with a nanosecond laser to create microscale spikes. This system is capable of processing arbitrary areas uniformly in order to achieve low processing times and high efficiencies. A Gaussian beam profile was selected to allow for secondary heating of the structure to anneal the previously formed spikes. This process is proposed to recrystallize the structure and remove the need for further chemical etching processes.

Chapter 2 describes the need of improving the utilization of renewable energy resource. The market is currently dominated by nonrenewable resources due to the low cost despite the disadvantages which include environmental concerns. The current renewable energy production in this country is low, but gradually increasing. Solar energy is a viable form of renewable energy that has the potential to produce enough energy to satisfy the need of the country. A current issue with harvesting solar energy is the high manufacture costs to build these devices. Lasers can improve the efficiency and quality of these processes.

Chapter 3 briefly explains laser processing, relevant heat transfer mechanisms, and the characterization methods of the laser-processed samples. Laser processing includes the basics of laser operation, pulsed lasers and in particular the Nd:YAG nanosecond laser, as well the optical components that are used in these systems. Relevant heat transfer mechanisms such as ablation and melting are described to show the laser-material interactions. The laser processed areas were characterized with various tools that will be briefly described in this chapter. These tools include: optical spectrometer, electron microscopy, focused ion beam, and the Hoffman apparatus.

Chapter 4 will delve into the silicon solar cell and the operation of the solar cell will be explained. Current research done to enhance the performance of the silicon solar cell will be shown. Next, the experimental setup for laser-assisted surface texturing will be explained, followed by the corresponding experimental results. The experimental results include: process uniformity and arbitrary scan area, simultaneous laser annealing, a parametric study, and the effect of laser scanning speeds towards practical processing speeds.

Chapter 5 describes other energy related surface texturing applications to this process. Surface texturing of materials can increase the surface emissivity, which can be applied to heat exchangers and evacuated tube solar collectors. Surface texturing can also increase the surface area, which has several uses. An increase in surface area can be applied to the electrodes of fuel cells to improve the efficiency and lifetime. In addition, it can be used to enhance the production of biofuels, such as algae.

Chapter 6 gives a brief overview of the work presented in this thesis. Topics of possible future study are also described.

CHAPTER 2: UTILIZATION OF RENEWABLE ENERGY AND LASER-BASED ENERGY MANUFACTURING

A gradual shift is occurring between extracting energy from nonrenewable resources to renewable resources. Renewable resources include, but are not limited to: wind, flowing water and sunlight. Solar cells are being researched, developed and fabricated in order to convert the energy in light to power, in the form of electricity. One of the driving forces for the advancement of this technology is the hazards produced from the current nonrenewable resources and the advantages of renewable forms of energy, shown in section 2.1. Section 2.2 will show how the distribution of energy produced in the United States is slowly changing over time. A brief overview of the current solar cell technology will be provided in section 2.3. Section 2.4 will show the energy that can be harnessed from the sun.

2.1 Needs for Renewable Energy Resources

Energy production can be either renewable or nonrenewable. Renewable energy can come in many forms, including wind, hydroelectric, geothermal, biomass and solar. Nonrenewable energy, also known as fossil fuels, requires extensive time to produce (300 million years or more).[8] Oil, natural gas and coal are all considered nonrenewable fuels.

Nuclear energy can exist as both a nonrenewable and renewable source of energy, depending on the material used. Uranium-235, a pound of which can generate more energy than 3 million pounds of coal, is a nonrenewable energy source because it is found in nature.[9] On the other hand, Uranium-233 and Plutonium used in a process called fast-reaction nuclear power generation are considered renewable sources of energy since the processes produce larger quantities of Uranium and Plutonium than it uses.[9]

To a certain degree, every kind of energy harvesting device has a negative impact on the environment. For each case, a structure must be added to the environment where the resource is available. This structure must change the resource into a usable form of energy (i.e. electricity) or transport it to a facility where that conversion can take place. Each modification to the environment has the potential of causing harm to that location and its inhabitants.

Nonrenewable energy can cause additional environmental problems. The byproduct of creating nuclear energy is radioactive isotopes, which takes hundreds of years to decay to safe levels. Fossil fuels can cause undesirable effects to the environment, such as acid rain, smog and oil spills, as well as climate change. Climate change is caused by a release of excessive greenhouse gases from burning fossil fuels, which remain in the atmosphere and prevent infrared radiation from escaping.[9] Energy production from solely renewable energy will not prevent all negative environmental effects, but it will go a long way toward minimizing them.

2.2 Current Energy Production

The energy production in the United States is dominated by nonrenewable resources, and the shift away from these sources is occurring slowly. The figures below show energy consumption in the United States from 2003 to 2009.

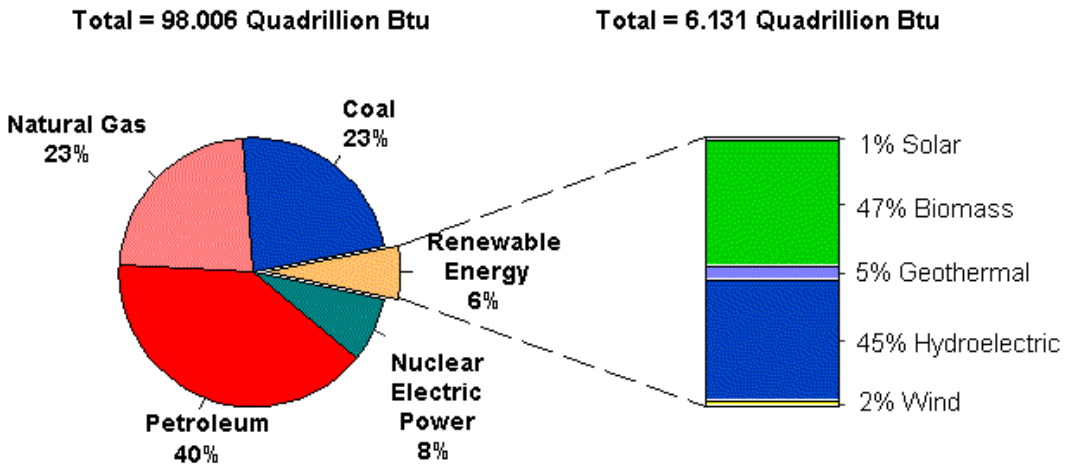

Figure 2.1: U.S. Energy Consumption in 2003[10]

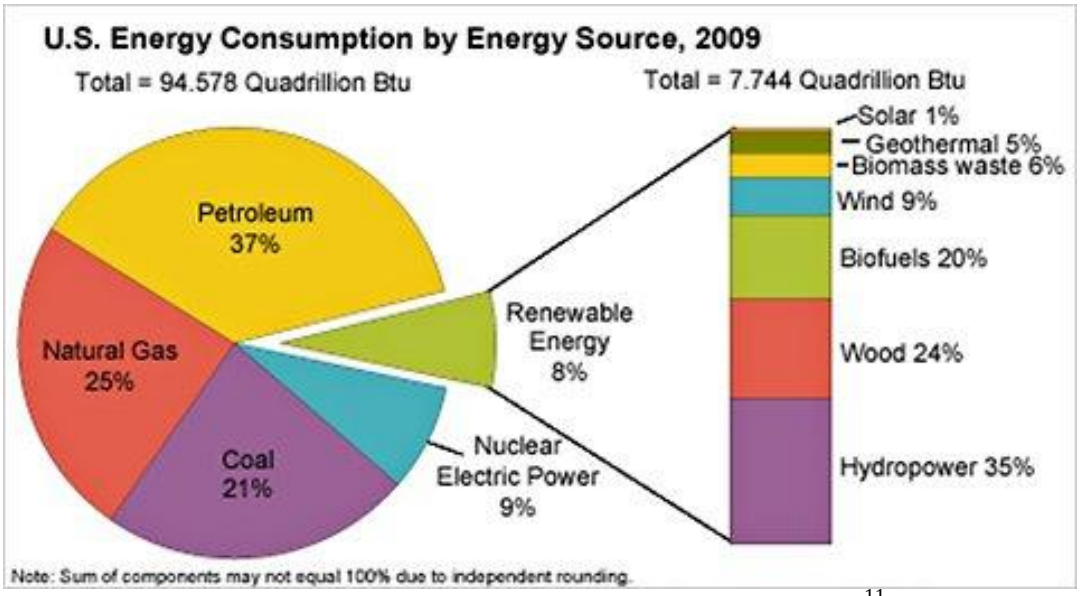

Figure 2.2: U.S. Energy Consumption in 2009[11]

The figures clearly show a 2% increase in renewable energy consumption compared to nonrenewable sources in a seven year period. This may not seem significant, but quantitatively it is an increase of 1.613 quadrillion BTU. During this expansion of renewable resources, solar energy has held a constant 1% of the renewable energy supply. It has increased 12% every year.[12]

Although current solar energy production accounts for less than 1% of the created energy in 2009, the possible application of this resource will be shown with the following example. The

amount of energy that can be delivered from sunlight varies depending on location and weather condition, but can be assumed to be 1 $\frac{kW}{m^2}$ for a clear day at noon.[13] If this energy could be collected with 100% efficiency for a year, 100 EJ (95 quadrillion BTU) would be generated. This would have satisfied the energy requirement for the United States in 2009. To achieve this amount of energy, about 3.24 Gm^2 of land would need to be covered with solar panels. The United States has an estimated area of 9.31 Tm^2 (2,300,000,000 acres).[14] If solar panels covered 0.0348% of the United States, they would generate enough energy to power the entire country. This quantity is a rough estimate and parameters such as location, duration of sunlight and corresponding change in sunlight intensity, weather conditions, material cost, maintenance and the efficiency of the solar panels as well as the mechanisms to transport the created electricity would need to be taken into account to find the true area required. Even with these limitations, the calculations show the potential and importance for continued research and development of technologies in this field.

2.3 Solar Energy as a Promising Renewable Energy Resource

The solar energy industry is driven by the goal to create the most efficient and least expensive solar cells. Both elements are critical parameters in this field. Efficiency is needed in order to harvest the maximum amount of energy and thus limit the number of solar cells needed. Cost is a factor because solar cells will not be successful in the long run if the expense of installing and running solar cells is greater than that of an alternative.

New solar cell concepts sometimes focus solely on improving the efficiency of the cells. The National Renewable Energy Laboratory (NREL) collects the findings on the progress that has been done to improve the efficiency of solar cells and compiles the information into tables. Version 38 was studied to gain insight on current methods of improving solar cell efficiencies. A few of these results will be presented below and can all be found in the "Solar cell efficiency tables (Version 38)."[15] The efficiency record is: 25.0% for crystalline silicon, 20.4% for multicrystalline silicon, and 19.1% for thin film silicon cells. Research is also being done on multijunction cells that take advantage of the different bandgap energy levels of certain materials. The design of these cells allows the optimization of absorbing energy from a larger range of wavelengths of sunlight. Materials besides silicon such as GaAs and CIGS thin films, are also gaining importance in continual research. Silicon is a popular choice, since it is the second most abundant element on earth.

Commercial solar panels must examine the entire process of material selection, fabrication, installation, warranty and lifetime. In order for the panels to be successful commercially, consumers must see economic benefit in investing. That being said, the efficiency of commercially available solar cells is typically lower than the most efficient solar cells that currently exist. In the market today, the efficiency of single-crystal silicon is around 20%, multicrystalline silicon is almost 14%, and thin film solar cell is over 11%[16]. The actual cost of such panels varies and depends on parameters such as the amount of energy needed and the location.

Designing solar cells with relatively high efficiency ratings is a good start. In order for such a design to be economically feasibility, it must be able to be manufactured quickly, in large

quantities and relatively cheaply. Fabricating high efficiency solar cells can be made at a lower cost since they can be made with less material. To accomplish these goals, fabrication processes must be developed and tailored to individual solar cell designs. This will allow the mass production of the solar cells to be optimized.

2.4 Energy from the Sun

Light from the sun comes in the form of photons, which contain discrete quantities of energy. Photons behave as particles as well as waves. The particle properties are induced from their mass and their speed. Photons travel at the speed of light ($3\times 10^{8}\,\frac{m}{s}$). The flow of an array of photons portrays their wave properties. The energy, *E*, which is stored in a single photon, can be calculated from the following equation:

$$E = \frac{hc}{\lambda} \tag{2.1}$$

In the above equation, *h* is the Planck constant ($4.135667516\times 10^{-15} eVs$), *c* is the speed of light in a vacuum ($299{,}792{,}458\frac{m}{s}$), and λ is the wavelength of the given photon.

Now that an equation for the amount of energy that can be delivered from the sun has been shown, the next step is to figure out the energy levels. In equation 2.1, there is only one parameter that can be varied, the wavelength. As wavelength decreases, the amount of energy in the photon increases. The figure below shows the variation in wavelength in light that reaches the Earth:

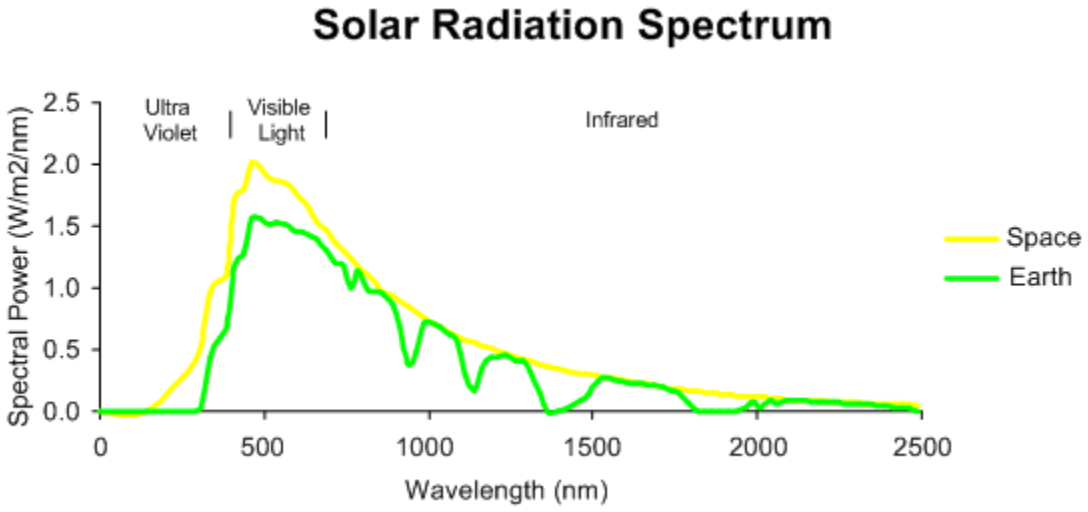

Figure 2.3: solar radiation spectrum[17]

The figure above shows which wavelengths have the higher spectral power, which correlates to a higher concentration of photons. Wavelengths in the visible spectrum seem to have the most photons. The figure shows the peak to have a wavelength of about 500 nm which would have an energy level of 2.48 eV.

CHAPTER 3: LASER PROCESSING AND LASER-MATERIAL INTERACTIONS

This chapter focuses on the operation and selection of lasers as well as their interaction with surface structures. Laser processing will be described in section 3.1. Section 3.2 will describe the relevant heat transfer mechanisms. Section 3.3 will briefly mention laser-based energy manufacturing. Section 3.4 will show the equipment that was utilized to characterize the processing areas.

3.1 Laser Processing

An integral part of these experiments is the laser. LASER is an acronym, which stands for Light Amplification by Stimulated Emission of Radiation[18]. The concept of a laser was devised in 1958. Lasers create waves of coherent light and amplify them to high intensities. These devices have various applications including the ability to alter the optical and physical properties of materials. This section will describe the basics of laser operation, the laser variant that will be used and the induced effects from laser processing.

3.1.1 Laser Basics

The structure of a laser contains three elements: the pumping source, the active optical gain medium and the optical resonator. The pumping source supplies energy to the medium in the form of electromagnetic waves and can be flashes of high intensity light, a gas discharge, or an electrical current.[19] The active optical gain medium amplifies the electromagnetic waves. For electrical current pumping source, the process begins with electroluminescence.[20] Electroluminescence is defined as light generated when current flows through a device under an electrical bias. Light created in this form only has a small spectrum of wavelengths. In particular, all classifications of lasers emit coherent monochromatic light.

Regardless of the method, the energy delivered form the pumping source allows electrons in the medium to move from the ground state to the excited state.[21] There are various orders of excited states that the electrons can reach depending upon the amount of energy transferred to them. The goal is to increase the population inversion, which is the ratio between electrons in the excited state to electrons in the ground state. A higher inversion would indicate a larger amount of energy stored by the electrons. Gradually the excited electrons move to lower orbitals by releasing energy by emitting photons. The photons have a specific wavelength that depends on the energy released as the electron moves to the lower orbital.

For some lasers, the active medium is a semiconductor[19]. Here, the energy from photons allows electrons to reach the conduction band. Excess electrons are lost due to recombination transitions which occur between an electron and a hole. These recombination transitions can be radiative as well as nonradiative. In order for a material to be effective as luminescent material, radiative transitions must be dominant. Recombination is desired since radiative transitions emit photons, which are seen as light. Semiconductors with a direct bandgap are ideal for lasers due to their radiative recombination.

Radiative transitions occur through injection electroluminescence. Here, minority carriers are injected into a semiconductor near the p-n junction. When an electrical bias is applied, the electrons are provided enough energy to cross the p-n junction. At this point, photons are emitted

in the form of light as electrons lose energy and move from the conduction band to the valance band.

The photon being emitted may induce a similar photon to be emitted in addition to the first. This is known as stimulated emission.[21] Photons induced from stimulated emission will have the same frequency and direction as the initial photon.

The intensity profile of a laser beam is determined by the geometry of the laser cavity.[22] The beam profile is classified as TEM_{nm} modes. Transverse Electromagnetic (TEM) modes do not allow electric or magnetic fields in the propagation direction.[23] The individual modes are denoted by denoting the horizontal nodes (n) and vertical nodes (m). The highest degree of symmetry is found in TEM_{00} and is known as a Gaussian profile.

Two highly reflective mirrors are used as an optical resonator.[21] These mirrors are aligned toward the medium on either side of the medium, coated to reflect photons with specified wavelength and phase. As the photons move back and forth across the medium, they stimulate more photons to emit through stimulated emission. The distance between the mirrors affects the rate of emission.

One of the mirrors is coated such that although it reflects the photons, some are allowed to pass though.[19] The electrons that pass through the mirror are known as the laser light. Design of the optical resonator can be done to only allow amplification of TEM_{00} mode. Higher-order modes have severe losses due to scattering from high divergence. Only frequencies above the population threshold and within the frequency span can be amplified.

The intensity at a given point can be found with the following equation:

$$I(r,t) = I_{pk}(t)\exp(-\frac{2r^2}{\omega^2}) \tag{3.1}$$

The above equation is dependent upon the peak intensity, I_{pk}, the time, *t*, the radial coordinate, *r*, and ω which shows the radius in which the peak intensity drops by a factor of $\frac{1}{e^2}$. For pulsed lasers, the total energy delivered from each pulse can be found from:

$$E_{pulse} = \int_{-\infty}^{+\infty}\int_{0}^{+\infty} I(r,t')\, 2\pi r\, dr dt' \tag{3.2}$$

The time of each pulse in equation 3.2 is denoted by t'. Pulse energy can be normalized based on area and this parameter is known as pulse fluence:

$$F = \frac{E_{pulse}}{\pi\omega^2} \tag{3.3}$$

The emitted laser light has three distinct properties the light is monochromatic, coherent (each photon's wave front moves in synchronization) and directional, with a relatively tight beam spot size and high intensities.[21]

3.1.2 Pulsed Lasers

Pulsed lasers are able to transfer energy to a work piece in a short amount of time. They can provide localized heating to texture surfaces, which allows for the geometric topography of the surface to be controlled.[3] Pulsed lasers are able to precisely machine dimensions smaller than

a micrometer on materials, such as silicon, that would be difficult to machine otherwise.[22] Such a structure is critical for the optimization of light trapping.

Pulsed lasers send energy to the material in pulses of relatively short time durations. Nanosecond lasers have pulse durations on the order of nanoseconds while femtosecond lasers have pulse durations on the order of femtoseconds. These two variations of pulsed lasers interact differently with materials, which must be considered for laser processing.

The duration of the pulses from the femtosecond laser is a million times shorter than that of the nanosecond laser. This means that the resolution of the femtosecond laser is a million times greater than that of the nanosecond laser. The femtosecond laser requires fewer pulses for surface texturing.[3] The time duration of these pulses is so short that two effects occur. The first effect is that features smaller than the spot size of the laser beam are able to be machined precisely.[24] The second effect is that there is no heat affected zone, which is present for the nanosecond laser.[2] The heat affected zone allows for an area larger than the spot size to be affected by the laser. The penetration depth for the nanosecond laser is relatively large compared to the femtosecond laser. This is important when considering scaling this process to large scale fabrication since the modification of a larger volume allows for materials to be processed faster.

Nanosecond lasers are better when it comes to initial cost, since a nanosecond laser can be up to an order of magnitude cheaper than a femtosecond laser. Nanosecond lasers are also smaller and more compact in size. Even though femtosecond lasers have advantages over the nanosecond laser in quality, the nanosecond laser systems have their own advantages of larger working volume and smaller cost to produce results that are acceptable compared to the femtosecond laser but on a larger scale.

3.1.3 Nd:YAG Nanosecond Lasers

Nanosecond lasers allow for energy to be delivered in pulses on the time scale of a few nanoseconds. The Q-switched Nd:YAG nanosecond laser is of particular interest. Typically these lasers have: pulse durations between 7 and 10 ns, a wavelength of 1064 nm, power between 10 mJ and 1J and a repetition rate of 10 Hz.[19] Yttrium aluminum garnet ($(Y_3Al_5O_{12})_{13}$) crystals are doped with neodymium (Nd^{3+}). Nonlinear crystals can be added to alter the wavelength from 1064 nm to 532, 355, or 266nm. As the altered wavelength decreases, the efficiency of the process and the pulse-to-pulse stability decreases. This material achieves thermal stability and exhibits properties appropriate for short-pulse and continuous-wave laser operations, with outputs usually insensitive to temperature. These lasers are pumped by semiconductor lasers.

The pulse duration for nanosecond lasers is done by Q-switching.[25] The quality factor, *Q*, is the ratio of active medium stored energy and energy lost per oscillation. Q-switching occurs by pumping the active medium while the quality factor is low (high degree of energy losses). Physically, this is done by blocking the path between the two mirrors, increasing light scattering and reducing amplification. When the obstruction to the path is removed, the quality factor becomes high (low degree of energy losses). The pulse is released and the process repeats.

3.1.4 Optical Components

Special consideration must be given for all optical components that interact with the laser beam. Using materials and coatings not appropriate for the laser beam could distort the beam and lead to damage of the components. For the Nd:YAG laser with 1064 nm wavelength, quartz and

glass coated with an antireflection coatings optimized for this particular wavelength can be used as lenses.[19] Thin film antireflection coatings can lower the reflection to 0.01 even though issues with the transmission, thermal conductance, hardness, smoothness and chemical resistance of the coating play a role in its performance.

Lenses are used to decrease the spot size of the laser beam, which also increases the intensity. There are two important parameters of lenses. The beam's focal waist, ω_{02}, and the location of this diameter in front of the lens, z_2. For a Gaussian beam with circular cross section, focal waist and the location in front of the lens can be found from:

$$w_{02} = \frac{f\lambda}{\pi w_1} \tag{3.4}$$

$$z_2 = f + \frac{f^2}{2z_{R1}} \tag{3.5}$$

The above equations show four variables: the focal length of the lens, *f*, the wavelength of the laser beam, λ, the beam diameter at the lens, w_1, and the Rayleigh length before the lens, z_{R1}.

Another optical component is the mirror. Mirrors allow for the laser beam's trajectory to be manipulated to fit a given setup with minimized optical losses. A mirror contains multilayer dielectric coatings to increase the reflection to 0.99 for a particular wavelength.[19] Using a mirror not rated for a given wavelength with high intensity could have reflections lower then specified which would damage the material due to an increase in absorption.

3.2 Relevant Heat Transfer Mechanisms

The interest of this thesis is on the interaction of lasers with materials, in particular Silicon. Thermal equilibrium between the lattice and the electrons is achieved when the diffusion time scale is much greater than the relaxation time of picoseconds of energy carriers, and the characteristic length scale is much longer than mean free path of electrons. For nanosecond lasers, thermal equilibrium can be assumed, which allows classical continuum transport models to be used to describe the laser-material interactions.

Schematically, the laser-material interaction is shown below in figure 3.1:

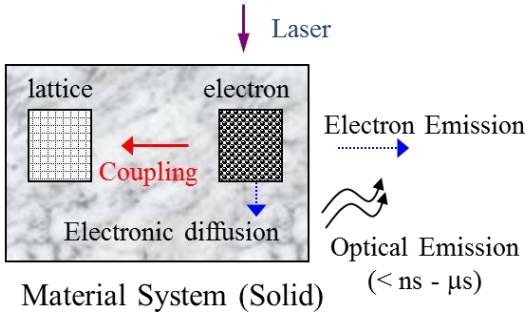

Figure 3.1: Laser-based heating mechanism

A laser provides energy to the structure. Part of the energy gets reflected, while the rest of the energy gets absorbed. The laser provides energy to electrons and, if the provided energy is

large enough, to the lattice structure as well. As the lattice gets more energy, the vibration experienced by the atoms increases, leading to structural modifications.

Energy from the laser beam is used to modify the material's structure[19]. Unfortunately, not all of the energy from the laser light is absorbed. The magnitude of energy absorbed is dependent upon the material's optical properties. In particular, the complex refractive index, $n^c = n - ik$, depends on laser wavelength and temperature of the material at that location.

The complex refractive index can be used to determine several useful parameters. The first of which is surface reflectivity. Silicon should have high absorption in order to be an effective material for solar cell application. Assuming zero transmission, knowing the reflectivity of a material will also shows the absorptivity. The equation to calculate reflectivity is:

$$R = (n-1)^2 + \frac{k^2}{(n+1)^2} + k^2 \tag{3.6}$$

Equation 3.6 assumes negligible changes in properties due to temperature. It also assumes a smooth surface. As the material is processed, the laser beam provides energy that induces a thermal gradient across a heat-affected zone. This creates surface texturing dependent on the depth, which changes the complex refractive index of the material. Since the reflection is a function of the refractive index of the material, both the reflection and absorption are affected by the modifications. As surface texturing increases, so does absorption. However, for silicon, at a given point in time when melting of the material is induced (during the molten phase) the reflection is increased due to thermal instability, thus lowering the absorption at that instant.

Tabulated optical properties of materials can be found in literature. These results refer to samples with prepared surfaces, usually in vacuum. Oxides and defects on the surface can affect absorption.

For roughness greater than λ/10, surface light scattering makes the determination of absorption more complicated. For semiconductors, including Silicon, the true absorption is higher due to the generation of free carriers as laser energy increases.

The absorbed energy can only penetrate so far into the material. This thickness is known as the absorption depth, d_{abs}, and can be calculated by:

$$d_{abs} = \frac{1}{\alpha} = \frac{\lambda}{4\pi k} \tag{3.7}$$

The above equation is dependent on the inverse of the absorption coefficient, $\propto$. The absorption depth in equation 3.7 can also be found by utilizing the wavelength, λ, and the imaginary component of the refractive index, *k*.

Another important parameter is the volumetric energy intensity absorbed by the material. Taking into account the assumptions previously mentioned, the volumetric energy intensity absorbed, Q_{ab}, becomes:

$$Q_{ab}(x,y,z,t) = (1-R)I(x,y,t)\alpha e^{-\alpha|z|} \tag{3.8}$$

In equation 3.8, z is the depth at which the absorption is being analyzed. Equation 3.8 is only valid during the pulse duration ($0 < t < t_p$), where t_p is the pulse width. If the pulse is not interacting with the material, $Q_{ab} = 0$. According to Beer's Law, this depth cannot exceed the absorption depth. It should be noted that nonlinear effects induced from steep thermal gradients affect the profile of absorbed energy.

Equation 3.8 represents a simplified equation since it assumes one dimensional heat transfer. Additional terms would be needed if the heat transfer was two dimensional axisymmetric or three dimensional. One dimensional heat transfer cannot be assumed if:

$$2d \ll \sqrt{\alpha t_p} \tag{3.9}$$

In the above equation, d is the beam spot size and t_p is the pulse width. Contrary to equation 3.8, in this case α is the diffusivity coefficient. For this system, the diffusivity coefficient of molten silicon is assumed to be approximately 10^{-4} (liquid metal) and the pulse width is approximately 10^{-8}. This makes the right side of equation 3.9 approximately 1 μm. As will be shown in section 4.3.1, the beam spot size is approximate 7.6 μm. By looking at equation 3.9, 15.2 μm is not less than 1 μm. Therefore one dimensional heat transfer can be assumed.

The volumetric energy density absorbed by the material can be coupled with the density, ρ, specific heat for constant pressure, C_p, and thermal conductivity, K, of the material through the heat-conduction equation to solve for temperature. The heat-conduction equation is:

$$\rho C_p(T)\frac{\partial T}{\partial t} = \nabla \cdot (K(T)\nabla T + Q_{ab}(\mathrm{x,y,z,t}) \tag{3.10}$$

The material properties are functions of temperature, but can be assumed to be constant to find an approximation. The material has a thickness, d, an initial temperature, T_0, and the beam is incident on the surface at $z = 0$. The initial condition for equation 3.10 is

$$\mathrm{T(t = 0)} = T_0 \tag{3.11}$$

Two boundary conditions are also needed to completely solve the differential equation in equation 3.10. These boundary conditions are shown in the following two equations:

$$K\frac{\partial T}{\partial z}|_{z=0} = h_{conv,u}(T,x,y,0,t) - T_\infty) + \varepsilon_{em,u}\sigma_{SB}(T(x,y,0,t)^4 - T_\infty^4) \tag{3.12}$$

$$K\frac{\partial T}{\partial z}|_{z=d} = h_{conv,L}(T,x,y,d,t) - T_\infty) + \varepsilon_{em,L}\sigma_{SB}(T(x,y,d,t)^4 - T_\infty^4) \tag{3.13}$$

These boundary conditions equate the conduction to the convection and radiation heat transfer components for both the upper and lower surfaces of the material. These equations depend on the coefficients of convective heat transfer, h_{conv} and emissivity, ε_{em} as well as the Stephan-Boltzmann constant, σ_{SB}, and the ambient temperature, T_∞.

Besides the absorption depth, another mechanism that allows heat to propagate through the material is the thermal diffusion penetration depth, d_{th}, defined as:

$$d_{th} = \sqrt{\alpha t_{pulse}} \tag{3.14}$$

$$\text{Where: } \alpha = \frac{K}{\rho C_p} \tag{3.15}$$

If $d_{th} \ll d$, the material can be considered semi-infinite. The laser radiation gets absorbed solely by the surface If $\frac{d_{abs}}{d_{th}} << 1$.

The heat conduction equation assumes that the laser beam is stationary in relation to the sample. This equation can be modified to account for scanning the laser across the surface. Assume the laser beam scans across the x direction, we can define:

$$\xi = x - Ut \tag{3.16}$$

Equation 3.16 is based on the location of the beam in the x direction, *x*, its speed, *U*, and the time for the beam to get there, *t*. Equation 3.16 can be used in the heat-conduction equation of 3.10 to get :

$$\frac{1}{\alpha}\left(\frac{\delta T}{\delta t} - U\frac{\delta T}{\delta \xi}\right) = \frac{\partial^2 T}{\partial \xi^2} + \frac{\partial^2 T}{\partial y^2} + \frac{\partial^2 T}{\partial z^2} + \frac{Q_{ab}(\xi,y,z,t)}{K} \tag{3.17}$$

If the processing length is long enough, the temperature field can be assume to be stationary with respect to (ξ,y,z).

Heat transfer induces phase change on the surface structure. This phase change can come in two main forms for these processes: melting and ablation.

3.2.1 Melting

During the heating phase, energy from the laser beam excites electrons and eventually the lattice structure. When enough energy has been provided, the solid begins to melt. Usually this transition occurs at a specific temperature known as the melting temperature, T_m. The energy deposition on the surface of the material and the corresponding melting morphology are effected by the laser induced and initial roughness.

For a Gaussian beam, the energy absorption and corresponding temperature field are not uniform. When the material melts, the shape of the molten pool is determined by material thermal expansion, the change in density upon melting, and the variation of surface tension, σ_{ST}, on the liquid. This form of dynamic flow is called capillary flow and can directly affect the surface topography. Three possible cases are shown below:

$$\frac{d\sigma_{ST}}{dT} < 0 \tag{3.18}$$

$$\frac{d\sigma_{ST}}{dT} = \frac{\delta\sigma}{\delta T} = \frac{\delta\sigma}{\delta C}\frac{\delta C}{\delta T} > 0 \tag{3.19}$$

$$\frac{DT}{Dt} = \alpha\nabla^2 T \tag{3.20}$$

Equation 3.18 shows the condition in which the surface is depressed. Equations 3.19 and 3.20 shows the surface extending outward. Flow of liquid is driven by the rapidly changing gradient of the surface tension from time-varying distribution of temperature and the concentration of oxygen, C. Graphically, these equation are shown below in figure 3.2:

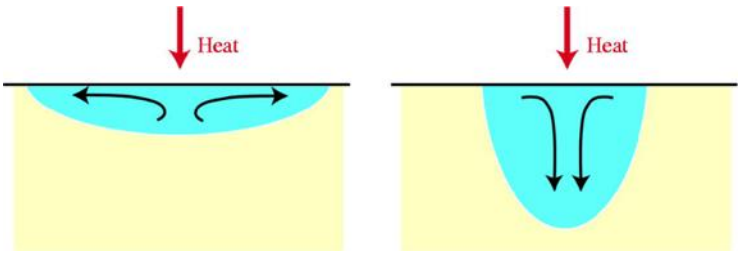

Figure 3.2: Capillary driven flow[26]

The left image in figure 3.2 shows equation 3.18, while the right image shows equations 3.19 and 3.20.

For nanosecond laser pulses, melting duration is on the order of tens of nanoseconds. Melt instability induces hydrodynamic motion from acceleration of molten phase from volumetric expansion upon melting. This can develop over hundreds of pulses.

The short pulses of a nanosecond laser allow for precise local heating and cooling of a structure. As mentioned in chapter one, these processes are necessary in order to decrease the reflection of photons in semiconductor materials, especially relevant for silicon. However, these processes, due to supercooling and rapid solidification, decrease the homogeneity of the structure and add defects to a point where the structures behaves more like amophorous silicon than polycrystalline or monocrystalline silicon. This is shown by less favorable electrical-transport characteristics of the material. A goal of post-processing of silicon in this manner is to recrystallize the structure on the microscale, thus increasing the electrical-transport characteristics of the material by improving the rigidity and homogeneity of the structure. This can be done by laser annealing.

3.2.2 Ablation

As previously mentioned, laser light induces vibrations in the lattice structure. Lattice vibrations can cause atoms on the surface to break away. This material removal process is known as ablation. When bulk material is removed, it goes to the vapor phase, known as the ablation plume.

There are several types of ablation including hydrodynamical and exfoliational. Hydrodynamical ablation is when micrometer size droplets are released from the surface during the molten phase. Exfoliational ablation is material removal in solid flakes. Separation of flakes occurs when defects in the surface structure absorb energy and cause the material to break away.

In general, thermal vaporization occurs when material is release from a heated surface as it melts to a liquid. To reiterate, since a nanosecond laser is being used, thermal equilibrium is established. Vaporization is easier to induce than surface melting with no ablation. For a surface absorber, defined as $\frac{1}{\gamma} << \sqrt{\alpha t_{pulse}}$, an energy balance can be used to estimate the material-removal depth, d_{abl}:

$$d_{abl} = \frac{(1-R)(F-F_{sh})-q_{loss}}{\rho C_p(T_{bp}-T_0)+L_{sl}+L_{sv}} \tag{3.21}$$

In the above equation, *s* denotes solid phase, *l* denotes liquid phase, *v* denotes vapor phase, and F_{sh} is fluence loss due to plasma shielding. Equation 3.20 is more accurate for short pulses. Longer pulses have more significant conduction losses. For laser intensities < $10^8 \frac{W}{cm^2}$, there is negligible energy absorbed by previously evaporated particles, thus vapor phase can be considered to be transparent.

Initially, when there is laser light incident on the surface, some of the energy is absorbed, and some is reflected. As the time the laser beam is bombarding the surface with energy increases, melting occurs. After that, vaporization begins. The ejected particles in the vapor can ionize, creating high density that absorbs some of the laser light before it hits the surface. This is known as plasma shielding, thus complicating the analysis.

3.3 Laser-based Energy Manufacturing

As in all aspects of manufacturing, solar cells must be fabricated quickly, at high volume, low cost and maximized efficiency.[27] The cost of production decreases as efficiency increases. The ultimate goal is to get the cost low enough so that solar cells can compete economically with nonrenewable resources.

Lasers are ideal for manufacturing processes due to their speed and precision. Lasers can be used for various processing techniques for crystalline silicon solar cell applications[28,29,30] including: edge isolation, laser fired contacts, wafer marking, laser grooved buried contacts, selective dielectric removal, laser doping, wrap-through, singulation, wafer marking, texturing, and hole drilling.

For example, it has been shown that 3,000 holes with a diameter of 50 μm can be drilled into silicon solar cells every second.[31] These holes can be used to move the electrical contacts from the front of the cell to the back, increasing the area for absorption of sunlight.

Edge isolation from lasers can be used prevent recombination at edges to enhance efficiency.[29] Lasers can be utilized due to their small spot size to maximize the active area of the cell. Lasers can also be used for laser grooved buried contacts. In this case, lasers mill out material such that the majority of the electrode is below the surface, maximizing the surface area for the semiconductor. Laser induced wafer marking allows for long-term identification of solar cells.

One of the reasons the cost of solar cells is so high is that current practices include pressing the electrical contacts onto the cell and then heating it in a furnace to make the connection.[31] Silicon breaks during this process, which increases the cost. Lasers can be used to selectively heat the contact to solder it, allowing for zero mechanical stress and a sufficiently lower percentage of solar cells that break.

Laser processing can be applied thin film solar cells.[28,30,32] Localized heating allows for precise laser scribing to minimize the so-called dead area of solar cells. Laser processing can also be used to recrystallize the relatively cheap polycrystalline silicon to achieve higher efficiencies. Pulsed lasers can be used to deposit photovoltaic materials onto a substrate to create a thin film photovoltaic cell.

In order for lasers to be applicable to industry, these processes must be performed quickly. For that to occur, either the part must be moved to change the relative location of the laser beam, the laser beam diameter must be increased to cover the entire part, or the laser beam itself must be moved. The first option is decent but undesirable since it would be relatively slow motion. The second option is not good since it would be difficult to increase the beam size to any size the manufacturer wanted and it would be hard to keep the energy level constant through that spot size. The third option allows for the laser beam to be moved quickly and it seems like the best choice.

This research focuses on a combination of laser texturing and scanning. Laser texturing allows for the absorption of solar cells to be enhanced in a controllable manner. The scanning allows for the time it takes to complete the process to be minimized.

3.4 Characterization Methods for Laser-processed Samples

After the samples have been processed, there must be a way to analyze the results. Four techniques were used. A spectrometer was used to measure the specular reflection to give insight into the absorption of the silicon. A Scanning Electron Microscope (SEM) and a Focused Ion Beam (FIB) was used to see the structures on the microscale, and a Hoffman Apparatus to measure electrolysis.

3.4.1 Optical Spectroscopy

A spectrometer is used to measure reflection. The USB4000 from Ocean Optics was used for these experiments. A halogen light source shined a beam of light onto the sample. Even though the actual spectrometer used is different, an example of the setup is shown in the following figure:

Figure 3.3: Spectrometer Setup[33]

The spectrometer comes with a program called SpectraSuite, which is used to obtain the reflection data. The program needs to know what the worst case is and what the base case is in order to calculate the reflection on a random processing area. The worst case is found by removing the light source and recording the data. The best case is found by putting a mirror in front of the light source detector. In this case a mirror with a 90% reflection was used.

Reflection off a smooth surface is known as specular reflection while reflection off of a rough surface is known as diffuse reflection.[34] Specular and diffuse reflection is shown graphically in figure 3.4 below:

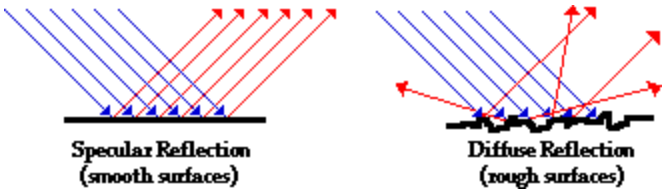

Figure 3.4: Specular and Diffuse Reflection

For specular reflection, light follows the law of reflection; light reflecting off a surface will have an angle of reflection equal to the angle of incidence with the surface. Diffuse reflection occurs when a surface is rough on the microscale. In this case, the light gets reflected in many directions.

The spectrometer setup used is designed to measure specular reflection, which is ideal for flat surfaces. Unprocessed silicon is the closest the material will be to become smooth on the microscale. After laser processing, the surface becomes rough on the microscale. The degree of surface texturing depends on various parameters, which will be shown in Chapter four. The reflection becomes diffusive and specular reflection measurements can no longer be used to see the total reflection. Due to constraints, total reflection was not attainable. Specular reflection is measured and can be used to determine relative changes in reflection. It should be noted that the reflection measurements here cannot be used to find the enhanced absorption of the processed areas.

3.4.2 Electron Microscopy

The Scanning Electron Microscope shines a focused beam of electrons onto a sample in a raster scan fashion, collecting secondary electrons to describe surface information.[35] On the other hand, the energetic electron beam can induce emission of x-rays from the specimen, offering Energy Dispersive X-ray spectroscopy (EDX) for elemental analysis.

3.4.3 Focused Ion Beam

The Focused Ion Beam uses gallium ions to take an image of the surface as well as perform precise machining.[36] At low primary beam currents, the gallium ions beam ejects a small amount of material from the surface as secondary ions, neutral atoms, or secondary electrons. A raster scan is used to scan the beam across the surface. The signal from the secondary ions, neutral atoms and secondary electrons gets collected and forms a signal. At high primary beam currents, a large amount of material can be precisely milled on the submicron scale.

3.4.4 Hoffman Apparatus for electrolysis

The Hoffman Apparatus is used to produce gases from liquids.[37] To operate, the device is filled with a liquid. Two electrodes are connected to a power supply inducing gases to bubble off of the electrodes. The two glass tubes that mount the electrodes are graduated cylinders such that the production of gases can be measured if the valves are closed. A picture of a Hoffman apparatus is shown in figure 3.5 below:

Figure 3.5: Hoffman Apparatus

In this case, a mixture of potassium hydroxide and water is used as the liquid to produce hydrogen and oxygen. The voltage of the power source was set to 4 V and the device was allowed to run for five minutes. By measuring the change in potassium hydroxide in each graduated cylinder, the amount of hydrogen and oxygen produced can be seen. This was conducted while different samples as electrodes to see the effects of surface texturing on the production of hydrogen and oxygen.

CHAPTER 4: LASER TEXTURING OF SILICON FOR ENHANCED LIGHT TRAPPING IN SOLAR CELLS

This chapter focuses on solar cell operation and the experiments performed on silicon. Section 4.1 describes the operation and variations of solar cells. Current silicon texturing for enhanced light trapping will be shown in section4.2. Section 4.3 describes the experimental setup. The results of the experiments for silicon are shown in section 4.4. Section 4.5 will give a brief summary

4.1 Introduction to the Solar Photovoltaic Cell

A photovoltaic cell (solar cell) is a device that absorbs the energy stored in sunlight and converts it into electricity. Typically, many of these cells are wired together in series and parallel to obtain the desired voltage and current output. The cells are packaged together in a frame to keep the entire structure rigid. A sheet of glass is added that protects the cells from the environment while allowing most, if not all, of the light to transmit through to the cells. The most important component in these cells is the semiconductor. Without it, electricity would not be generated. The following explanation will focus on how this device works with silicon as the semiconductor. The explanation holds true for other semiconductors as well.

4.1.1 Structure of Silicon

The element of Silicon has an atomic number of 14. For a neutral silicon atom, there are 14 protons, 14 neutrons, and 14 electrons. The electrons are grouped into three separate energy levels as shown below in figure 4.1:

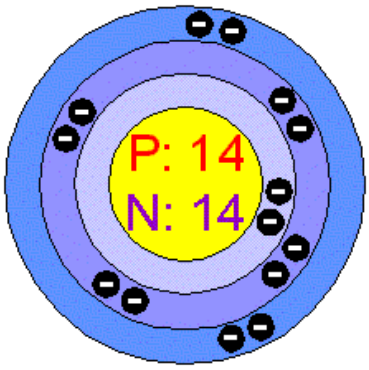

Figure 4.1: The atomic model of silicon[38]

The first two energy levels are completely full. The third energy level only has four electrons and is known as the valance band. This is only half the electrons required for the valence shell to be full.

The crystal structure of a material is comprised of a collection of atoms that can be repeated throughout the crystal, which is known as the primitive cell. The primitive cell for silicon has a diamond lattice structure, which can be thought of as two interpenetrating face centered cubic lattices.[26] Each silicon atom shares an electron from its valance band with four

equidistant atoms. This geometric arrangement of atoms forms a tetrahedron, shown below in figure 4.2:

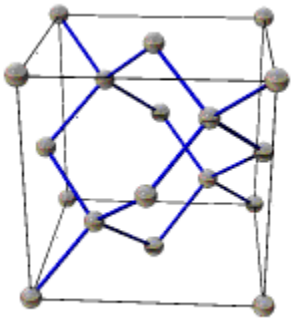

Figure 4.2: Diamond lattice structure[39]

The ability of a material to conduct electricity can vary. For a conductor, electrons in the valance band are able to move freely about the structure with the addition of as little heat as available at room temperature.[40] This continual motion of electrons allows metals to conduct electricity well with low resistance. In an insulator, electrons are bound to atoms and have a high resistance to electrical current. It is much harder for electrons to move freely in an insulator.

The semiconductor's ability to conduct electricity lies in the middle of conductors and insulators. Initially, the electrons in the valance band are bound to atoms. As energy is added, electrons are able to break away from the atoms and move freely through the crystal. A set amount of energy must be given to allow an electron to move from a valance band to a conduction band, where it can move freely. In between the highest valance band and the lowest conduction band exists an energy gap where electrons cannot be found.[26] For silicon, the energy needed for an electron to cross the energy gap is 1.12 eV at 300 K and 1.17 eV at 0 K. This means that at room temperature, if 1.12 eV is given to an electron, it will be able to escape the atom it is bonded to and move to the conduction band. As the electron is set free, it creates a hole and the silicon atom becomes a positive ion. This positive ion will now seek an electron to fill the vacancy.

Besides the valence band and conduction band, there are two important terms for a semiconductor. The Fermi level is defined as indicating the potential energy of an electron in a solid structure. The level falls in between the conduction and valance bands. This level changes when the structure is doped with a foreign element. The Fermi level can determine the density of electrons and holes in the structure. Silicon has an indirect bandgap. This means that in order to go from the highest valence band to the lowest conduction band, heat must be added. Heat provides the momentum to go from one maximum to a minimum which is not aligned.

For a crystal made entirely silicon, each electron in the valance band is covalently bonded to two atoms, allowing very few electrons in the conduction band. This quantity can be increased by doping the silicon with impurities as shown in the next section.

4.1.2 Doped Silicon

Doping is the process in which impurities replace silicon atoms in the crystal structure. This is done to increase the ease in which electrons can move freely, thus increasing the flow of electricity. Too few impurities will not make a significant change while too many can lead to a change in the dominate material behavior. The number of impurities is measured in parts per million (ppm). Typically, for doped silicon, there can be between 1 and 10 ppm.[41] There are two different types of doping: n-type and p-type. The figure below shows three configurations. The first case (a) shows pure silicon. The second case (b) shows an example of n-type doping. The third case (c) shows an example of p-type doping.

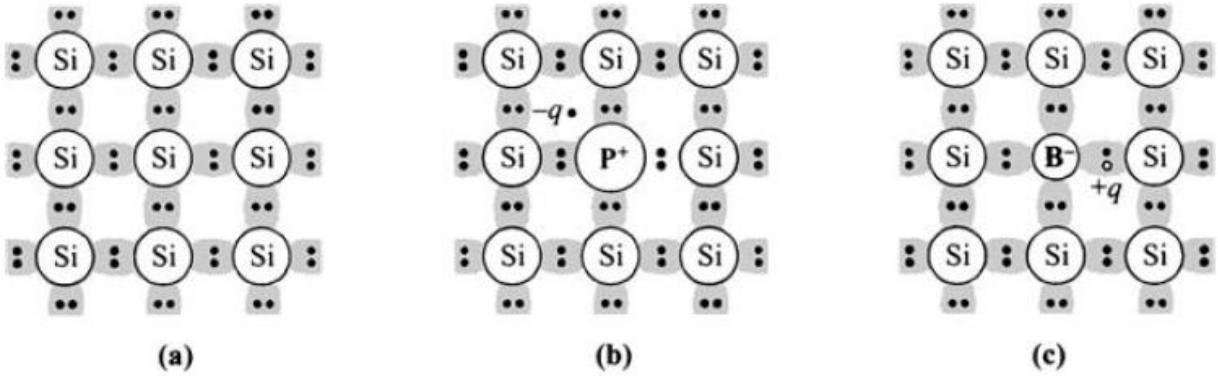

Figure 4.3: Bonding in a silicon semiconductor. (a) pure silicon. (b) n-type silicon with Phosphorus impurity atoms. (c) p-type silicon with Boron impurity atoms.[42]

N-type silicon (figure 4.3b) can be made by adding an impurity to the crystalline structure of silicon that has five valance electrons. In this case, the atom is covalently bonded to the nearest five silicon atoms, just as the silicon atom it replaced would have done. The difference is that now there is an extra electron that can be used to fill the holes created when electrons move from the valence band of an atom to the conduction band. The extra electrons make the charge of the structure negative, hence the term n-type. A typical impurity is Phosphorus.

P-type silicon (figure 4.3c) has the opposite effect when compared to n-type silicon. Here, the impurity atom has three valance electrons instead of four. This means that one of the four bonds that the impurity atom and resulting silicon atom share is missing. A hole is created at each impurity atom. When an electron is close enough to this hole, it will be attracted to the atom and will fill the hole in order to achieve neutrality with a full valance shell. The lack of electrons in some of the atoms leads to the charge of the structure to be positive which defines p-type silicon.

4.1.3 Silicon based Solar Cell

The ability to absorb light and transform it into energy in the form of electricity for the silicon solar cell begins by contacting n-type silicon to a layer of p-type silicon.[43] When this occurs, some of the excess electrons from the n-type silicon move to the holes of the p-type silicon. This only happens in the volume of p-type and n-type silicon that is relatively close to the area of contact.

The motion of electrons allows the atoms in the p-type silicon to make the necessary bonds to attain eight valance electrons. The part of the n-type silicon that loses the electrons becomes positively charged from the loss of electrons while the corresponding p-type silicone becomes negatively charged from the addition of electrons. This charged region forms an electric field that acts as a barrier for electrons. Only electrons with sufficient energy are able to cross over this region, which is known as the p-n junction.

When light hits the cell, the photons are absorbed by the electrons. This increase in energy can knock electrons loose in both the p-type and n-type silicon. Electrons are able to move to the conduction band when enough energy is provided that they are able to cross the band gap. Relatively, there are more electrons in the conduction band of n-type silicon due to the extra electrons provided by the doping. When equilibrium is achieved, electrons in the conduction band of n-type silicon have less energy compared to electrons in p-type silicon. This is due to more collisions occurring, which cause a loss of energy between a greater number of electrons. The higher energy of electrons in the p-type silicon increases the probability of electrons to cross the electric field barrier, which further increases electrons in the n-type silicon. This is the premise of a diode, where current can only flow in one direction.

Solar cells differ from diodes by the addition of a wire that connects the n-type and p-type silicon. Electrons from the relatively high concentrated n-type are able to move to the p-type without having to gain enough energy to go over the electric field barrier. This wire can be attached to an external system. In this case, the flow of electrons creates a current that does work. Thus, light is absorbed and creates a current that provides electricity for other uses, as shown in the following figure:

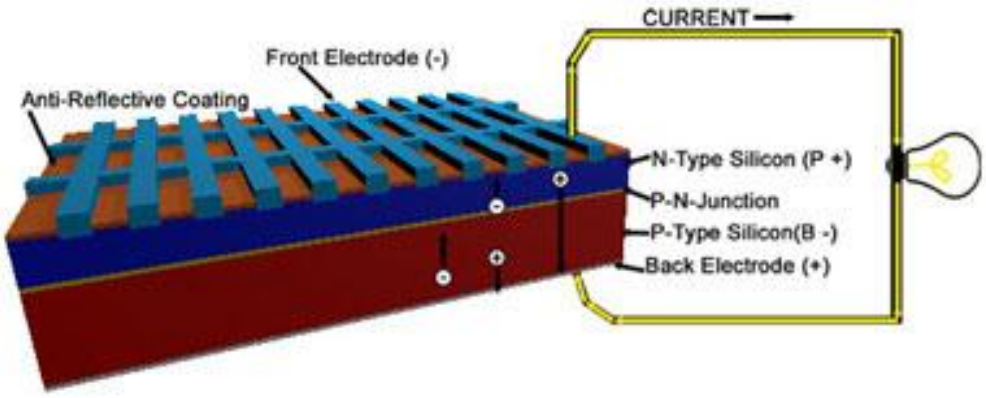

Figure 4.4 Setup of a typical solar cell[44]

The above figure shows the n-type and p-type silicon, as well as the relatively thin p-n junction. The antireflective coating is added to the top of the cell to decrease the intrinsic reflection of silicon. The front electrode collects the electrons from the n-type silicon and transports them to the exterior circuit. The size of the front electrode requires optimization, since a surface area that is too large would not allow enough photons to reach the silicon. On the other hand, because each electron moves with random motion, a surface area too small would not be able to sufficiently reach the maximum number of electrons. The current flows through the

external circuit symbolized by the light bulb. The external circuit can provide power to any external system. The circuit leads to the back electrode, which evenly distributes the electrons to the p-type silicon.

An important feature of a solar cell is its ability to work continuously for many years as long as there is an input of light. During this process, when electrons go to the conduction band, they create a hole and move in random directions until they find one to fill. The electron can fill a hole near where it was excited, or fill a hole by going over the electric field barrier or going through the wire. When it finds a hole to fill, the electron is ready to go into the conduction band again by an increase in energy from another incoming photon. This allows the process to be repeated.

4.1.4 Silicon Variants

The previous sections described the properties of silicon and how this material is used in devices such as solar cells. What was not mentioned was how the characteristics of the silicone affect the overall performance. Different types of silicon solar cells are created based on the type of silicon used. Section 1.3 gave some examples of efficiencies for several different silicone structures. The monocrystalline silicon was shown to have the highest efficiency, which is attributed to its structure.

The crystal structure of Silicon that was defined in section 4.1.1 shows a monocrystalline structure. High-purity silicon is melted and allowed to cool slowly.[45] At the same time, it is in contact with a single crystal "seed" which allows the fabricated silicon to adopt the crystal structure of the single crystal. The primitive cell is repeated continuously throughout the structure without defects. The atoms are aligned into rows, which is optimal for the ability of photons to excite electrons.[15]

Polycrystalline (multicrystalline) silicon is another form of silicon that is used in solar cells. Again, silicon is melted and allowed to cool, this time forming multiple crystals within the structure. The rate at which the Silicon cools determines the size of the crystals. Larger crystals present fewer grain boundaries, making the structure closer to monocrystalline silicon. The quality of the silicon that is melted can be of lowered quality compared to monocrystalline silicon. Solar cells produced with this material are typically cheaper than monocrystalline silicon but at the cost of reduced efficiency.

Amorphous silicon is another variant of silicon, in which there is no crystalline structure. The silicon atoms are randomly oriented and contain various defects.[47] Some atoms lack nearby atoms with which to bond. In this case, when electrons are excited, they go to fill the valance band of these atoms instead of generating a current. Hydrogen impurity atoms can be added to attach to the atoms that are missing bonds, allowing excited electrons to add to the current. Amorphous Silicon is typically used in applications with low power requirements.

Another variant of silicon is in thin film solar cells. The purpose of thin film solar cells is to be able to produce cells as cheaply as possible. A typical solar cell uses silicon with a thickness between $100\mu m$ and $300\mu m$. Silicon used for a thin cell is on the order 1- 10μm.[46] Considering that silicon is the most expensive material of the solar cell, a reduction of required material by roughly two orders of magnitude significantly reduces the cost to manufacture and purchase a solar cell of this type. Since photons will not have a chance to travel as far through

the semiconductor (compared to a typical solar cell), the silicon material can be of lower quality.[3] The benefit of this is a reduction of cost. On the other hand, a reduction in thickness coupled with a lower grade of material decreases the chance that a photon can be used to send electrons to the conduction band, thus decreasing the efficiency. Overall, thin film solar cells are relatively cheap but at the expense of efficiency.

4.1.5 Alternatives to Silicon

Silicon is a natural choice as a semiconductor due to its abundance in nature, which leads to a relatively low cost. Other materials have been shown to work well for solar cell application. The added cost is justified by the increase in efficiency, requiring less material. III-IV semiconductors are of particular interest. The element in column III has three electrons while the element in column V has five electrons. There is an average of four electrons per atom, allowing these semiconductors to behave similarly to silicon. Doping these semiconductors allows for n-type and p-type variations as described for silicon in section 4.1.2.

A popular semiconductor material is gallium arsenide (GaAs). The bandgap of gallium arsenide is 1.43 eV. It has a direct bandgap compared to silicon, which has an indirect bandgap of 1.12 eV.[47] For direct bandgap, heat is not needed for an electron to move to the conduction band, as is required for indirect bandgap. Compared to silicon, gallium arsenide is resistant to heat, allowing it to operate normally at elevated temperatures. The absorption characteristics of gallium arsenide exceed the absorption of silicon. For optimal absorption, a few microns are needed for gallium arsenide compared to at least 100 microns for silicon. The biggest disadvantage of gallium arsenide is the cost. Gallium is a byproduct of smelting metals, and is rarer than gold. Overall, gallium arsenide is a potential candidate for thin cell solar cells.

4.2 Si Texturing for Enhanced Solar Light Trapping

This sub-section will focus on reiterating the current improvements in this field and the motivation for this work. Current manufacturing processes are designed to optimize performance of solar cells within reason. Silicon ingots are cut into wafers through wire sawing.[48] This process induces defects that reduce the mechanical strength, and increase surface recombination. Etching is used to remove these defects. An example of the effect of etching on silicon wafers is shown below in figure 4.5:

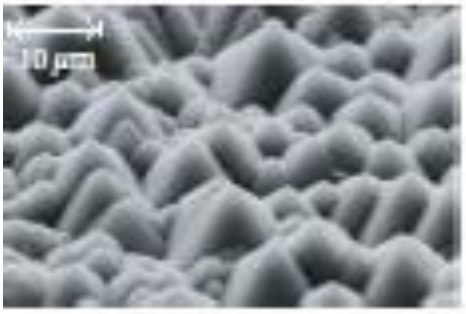

Figure 4.5: SEM of KOH etched silicon

A positive side effect of the etching is that it further textures the surface, reducing reflection. A schematic of surface texturing is shown below in figure 4.6:

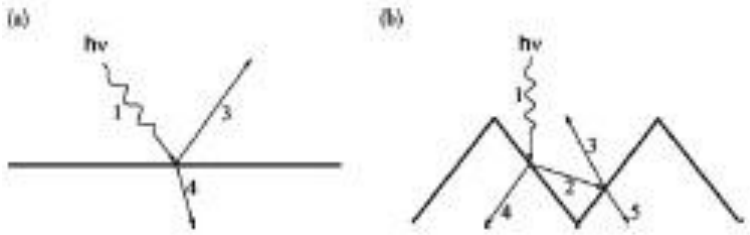

Figure 4.6: Photon interaction on: (a) a flat surface, and (b) a textured surface. The incoming light at 1 gets absorbed at 4,5 and reflected at 2 and 3.[4]

The above diagram shows surface texturing developed from geometric optics. Light has multiple chances to be absorbed into the material, which increases the optical path length of a photon.[3] Another way to analyze this situation is by looking at the refractive index for both air and silicon. The refractive index of air is much lower than that of silicon, which causes high initial reflection. When texturing occurs, the refractive index of silicone is based on the ratio of silicon to air, allowing the possibility of a smooth transition between the two refractive indices, creating a low reflection surface.[2] Thus, the effectiveness of the light trapping is affected by the geometry of the surface.

Surface texturing changes the morphology of the surface, inducing a change in the color. Research by various organizations and institutions has provided a basis for advancements in the creation of black silicon. It can be created by irradiation from femtosecond lasers by purely ablative processes.[5] Here, microgrooves are created by ablation to enhance light trapping, as seen below in figure 4.7:

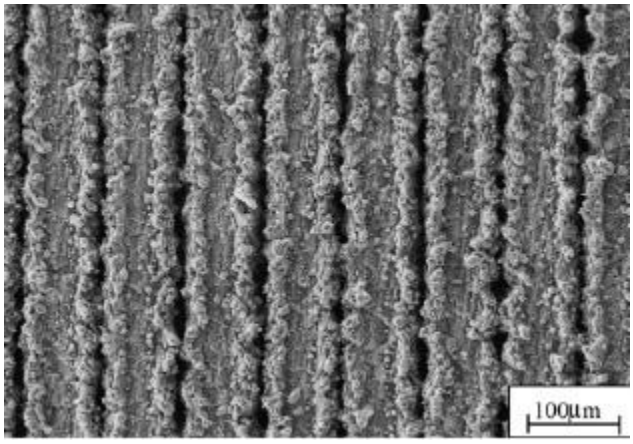

Figure 4.7: SEM image of microgrooves

This process is expected to decrease the overall performance of the solar cell due to loose structures being formed by the ablation, a decrease in the crystallinity of the surface structure and the rapid heating and cooling of the structure.

Black silicon can also be created by shining a femtosecond laser on a single spot for a large number of pulses[6]. This process creates spiked structures as shown below in figure 4.8:

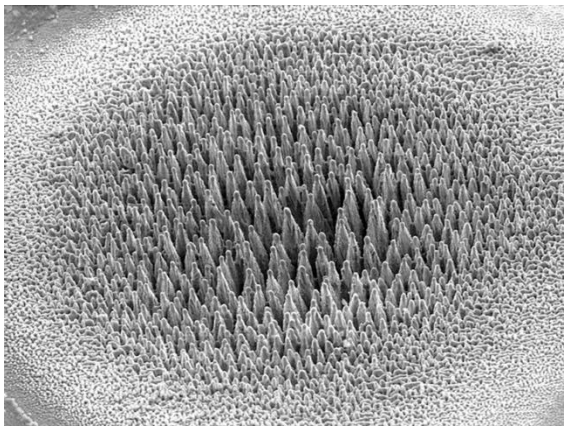

Figure 4.6: Black silicon from femtosecond laser processing[49]

The spiked structure grows from the center outward and traps light due to geometric light trapping. There are two main issues with this process in addition to the problems associated with microgrooves. This process requires an environment with an etchant, which is not ideal for manufacturing settings where working in air is the easiest and cheapest. Another issue is that the surface is not uniform, which provides limitations to the size of structures that can be processed at any given time. Black silicon has also been created by pulsing a surface with nanosecond lasers in a vacuum chamber.[7] The results were similar to the femtosecond laser case. The structured surface was not uniform and a chemical etchant was required to remove the defects form the laser processing.

This research suggests rapid scanning of a nanosecond laser with a Gaussian beam profile. The scanning would allow for an arbitrary area to be processed to enhance the uniformity and decrease the time required for processing. The Gaussian beam allows for secondary heating of the newly processed silicon in order to anneal the structure. Annealing would help to recrystallize the structure, improving the carrier diffusion length and removing the need for further processing through etching.

4.3 Experimental Setup for Laser-assisted Si Texturing

These experiments involved scanning a green Nd:YAG nanosecond laser (Yuco Optics) across a sample. The setup was designed to make the conditions repeatable. Section 4.3.1 will describe the system setup. The method used to focus the lens will be shown in section 4.3.2. Section 4.3.3 will describe the raster scan program utilized in these experiments.

4.3.1 System Setup

The setup was built on an optical table to ensure a flat surface as well as making alignment of the various components easier. A schematic diagram of the setup is shown below in figure 4.9 and a picture of the setup is shown in figure 4.10:

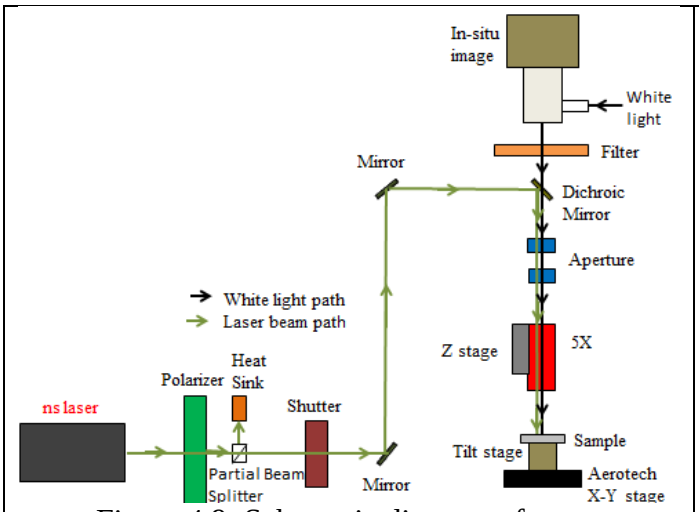

Figure 4.9: Schematic diagram of setup

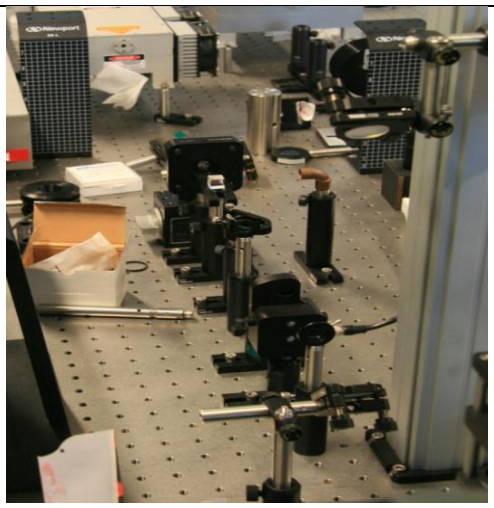

Figure 4.10: Picture of setup

The green Nd:YAG nanosecond laser has a wavelength of 532 nm. The pulse width and maximum power found from this laser depends on frequency. Table 4.1 shows these values for the frequencies used in the experiments:

Table 4.1: pulse width and maximum power for various frequencies

Frequency (kHz)	Pulse width (ns)	Maximum Power (W)
1	11	0.30
5	13	1.70
10	15	3.10
20	16	2.75

The laser light goes through a linear polarizer and corresponding polarizing beam splitter. The linear polarizer transforms the light into two laser beams with opposing polarizations. The polarizing beam splitter allows one of the beams to pass through while the other beam is reflected 90°. The beam that passes through propagates to the sample while the reflected beam is absorbed by the heat sink. By manually changing the polarization of the polarizer, the power of the laser beam can be controlled.

The laser light goes through a shutter. When open, the laser light passes through unaltered. When closed, the laser light is stopped from propagating any further. The shutter allows for the laser to be used only while the sample is being processed.

White light is used to illuminate the sample so that images can be taken in-situ with the 1.3 MP Aptina Color CMOS digital camera. A filter is used to prevent the high intensity of the laser light from damaging the camera. The white light and the laser light are coupled at a partial dichroic mirror. The white light passes through the mirror while the laser light is reflected. Two mirrors are used to align the laser light with the partial mirror. These mirrors are from Thor Lab and have a reflectance of 99% for this wavelength.

Two apertures are used to ensure the laser light is normal to the sample. If it is not, the two mirrors can be adjusted to realign the beam. The light passes through a 5x lens that is on a Z stage. The Z stage allows the lens to move vertically to adjust the focus onto the sample.

After the lens, the light reaches the sample. The beam spot size, *d*, can be found from equation 3.4 in section 3.1.1. An approximation can be made with the following equation:

$$d \approx \frac{2\lambda}{NA} \tag{4.1}$$

In the above equation, *NA* is the Numerical Aperture. For the 5X lens that was used, the numerical aperture is 0.14. According to equation 3.1, the beam spot size is about 7.6 μm.

The sample is attached to the tilt stage by double sided tape, which is mounted onto the Aerotech X-Y stage. There is no guarantee that the specimen is normal to the incident laser beam. To account for this discrepancy, the tilt stage can rotate in both the X and Y direction, allowing for a normal incident laser beam to be achieved with calibration. The Aerotech X-Y stage is used to scan the specimen back and forth relative to the laser beam.

4.3.2 Focusing of laser beam for desirable pattern size

In order to conduct a laser process over a given area, the laser beam must be in focus with the specimen at all times. Otherwise, the laser processing conditions will not remain uniform. To ensure this, the specimen must be normal to the incident laser beam, as mentioned in section 4.2.1, and the beam must be in focus.

A procedure has been developed for this purpose. A corner of the specimen is shot with the laser beam. The Z-stage is adjusted to bring the specimen damaged area into focus, seen from the camera. Next, the specimen is scanned in the x direction until the other corner is reached. The laser beam is shot again. This time the angle of the tilt stage in the x direction is changed until focus is reached.

The specimen is then scanned back to the first point, and small changes in the Z-stage and tilt stage are applied until the focus is regained. This is done for both points until they both are in focus. At this point, focus is guaranteed for the x direction for the entire sample. This process is repeated for the y direction.

4.3.3 Programming

All of the programming for the experiments was done through the A3200 Motion Composer from Aerotech. Most of the testing was done with modifications of a raster scan. An example of the code is shown below in figure 4.11:

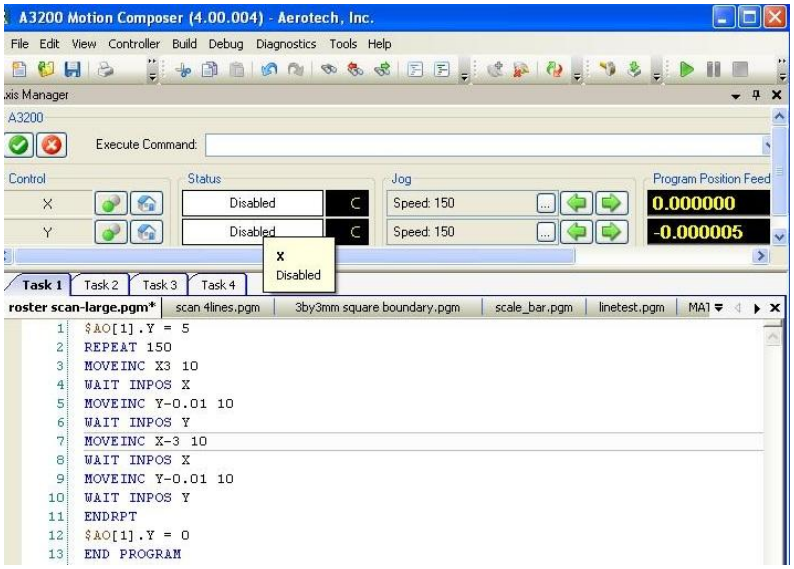

Figure 4.11: Example of raster scan code

The code above in figure 4.11 consists of 13 lines. Line 1 turns the shutter on and line 12 turns the shutter off. This allows for the laser beam to contact the surface only while the program is running. Line 2 is a while loop that has the program run 150 times. Line 11 denotes the end of the loop. Line 3 moves the motion stage in the x direction 3 mm at a rate of 10 mm/s while line 7 has the same conditions but it moves the stage in the negative x direction. Lines 5 and 9 move the stage in the negative y direction 10 μm at a rate 10 mm/s. Lines 4, 6, 8, and 10 has the program wait until the command before it is completed before it moves on to the subsequent lines of the program. Line 13 signifies the end of the program.

4.4 Experimental Results; Laser-based texturing of Silicon

A parametric study was performed on (100) P-type, boron doped monocrystalline silicon with a resistance between 1.65 Ωcm and 3.85 Ωcm. The sample was cleaned with methanol. Squares were processed via raster scan on the silicon surface with dimensions of 3 mm by 3 mm. For convenience and simplicity, the experiments were demonstrated in an environment of air. This has been shown to change the chemical composition of the surface structure by the creation of SiO_x.[5]

There are many factors that can affect the texturing of a material. These factors include material properties such as: absorption coefficient, thermal diffusivity coefficient, thermal expansion coefficient, melting point and evaporation point.[4] These factors also include parameters of the system such as: laser beam power, laser beam wavelength, pulse duration, pulse frequency, line spacing and scanning speed.

4.4.1 Process Uniformity for Arbitrary Scan Area

One of the main goals of these experiments was to be able to process a sample with arbitrary area uniformly. An example of the surface morphology after laser scanning is shown in a SEM image below in figure 4.12:

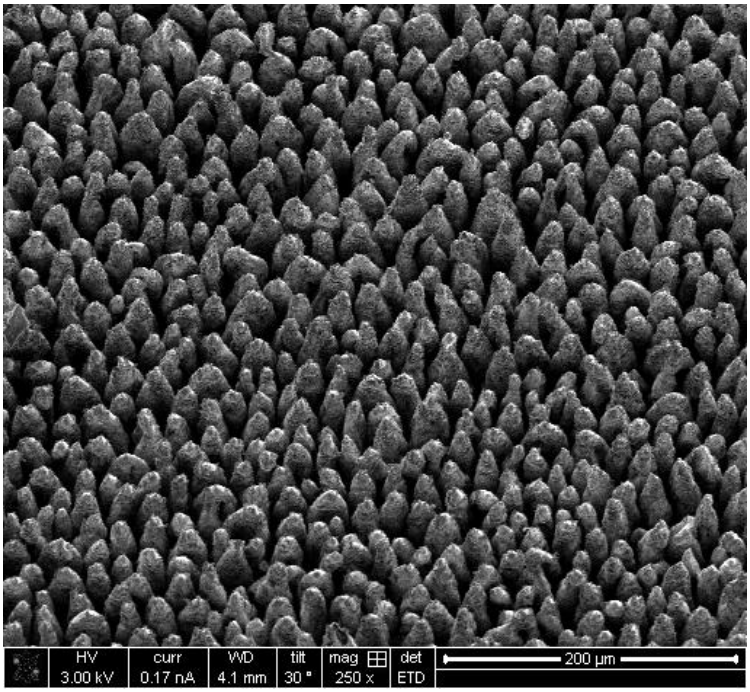

Figure 4.12: processed black silicon created with parameters: laser power of 3 W, line spacing of 10 μm, scanning speed of 10 mm/s, and a pulse frequency of 10 kHz

Compared to the black silicon created from a femtosecond laser shown in figure 4.8, the enhanced uniformity of the structure above is apparent. The laser processing induces ablation coupled with surface melting. Ablation initiates the spike structure. Surface melt instability induces the thermocapillary effect. The molten silicon flows due to a temperature gradient that depends on surface tension as it strives to minimize surface energy. The surface morphology improves absorption by increasing roughness on the microscale, but it also reduces the carrier length.[3,7]

The carrier length determines the capability of the device to transmit electricity, even though roughness is increased, while the current is decreased. The mechanisms used to absorb light in silicon depend upon the surface roughness. For smooth silicon (unprocessed), absorption comes from band transitions.[5] Surface structures larger than the wavelength absorb light due to multiple reflections.[3] On the other hand, surface structures smaller than the wavelength use transitions between the index of refraction for air and silicon to reduce reflection. Here, the spikes seem to be about 10 μm apart, which leads to a roughness much greater than the wavelength of sunlight. This then leads to enhanced absorption and a reduced reflection due to geometric optics. At the same time, the nanoscale protrusion helps to transition the photons from the low refractive index of the air to the high refractive index of the silicon.

The thermal capillary effect induces thermal diffusion. The length of diffusion, L, can be found from equation 4.2:

$$L \approx \sqrt{\nu t} \tag{4.2}$$

In the above equation, ν is the kinematic viscosity of the molten silicon and t is the time of the

molten period. The molten period for a nanosecond laser takes approximately 1 μs to cool. The kinematic viscosity can be derived from the Prandtl number:

$$\mathrm{Pr} = \frac{\nu}{\propto} \tag{4.3}$$

The Prandtl number is a dimensionless quantity defined as the ratio between kinematic viscosity and thermal diffusivity, $\propto$. Molten silicon can be considered to be a molten metal. This assumption makes the thermal diffusivity of molten silicon approximate to $10^{-4}\ m^2/s$, and the prandtl number is approximately 0.01. Equation 4.3 is used to calculate the kinematic viscosity to be 10^{-5}. Equation 4.2 shows that the diffusion length becomes 3.2 μm. The beam spot size, as shown in equation 4.1, is approximately 7.6 μm. Assuming thermal diffusion expands uniformly in all directions, the heat affected zone has a diameter of 14 μm.

A key characteristic of the structure is the periodicity. Periodicity can be defined in both the x direction (direction of scanning) and the y direction (direction of line spacing). For the x direction, spikes appear about once every 20 μm. The theoretical distance between pulses, *x*, can be found from the equation:

$$x = \frac{nv}{\nu} \tag{4.4}$$

Equation 4.4 contains 3 parameters: the number of pulses, *n*, the scanning speed, *v*, and the pulse frequency, *ν*. A single pulse with a scanning speed of 10 mm/s and a pulse frequency of 10 kHz, occurs once every micron travelled by the relative displacement between sample and laser beam. Considering the heat affected zone has a diameter of 14 μm, there is clear interaction between pulses that goes beyond a single beam spot size.

Spikes in the y direction occur about once every 17 μm, which is comparable to the heat affected zone is 14 μm. There must be an interaction of pulses in the y direction. Otherwise, the area shown in figure 4.10 would have an average of 300 spikes in the y direction instead of the 30 spikes actually created.

4.4.2 Simultaneous Laser Annealing for Improved Carrier Transport

The methods for creating black silicon that were shown in section 4.1.5 use various methods to achieve their goals. A common problem is the creation of loose structure that requires an additional step (chemical etching) in order to create acceptable solar efficiencies. To see the effect of line scanning, the processed area after the first scan, the third scan and the sixth scan are shown below for three variations in power:

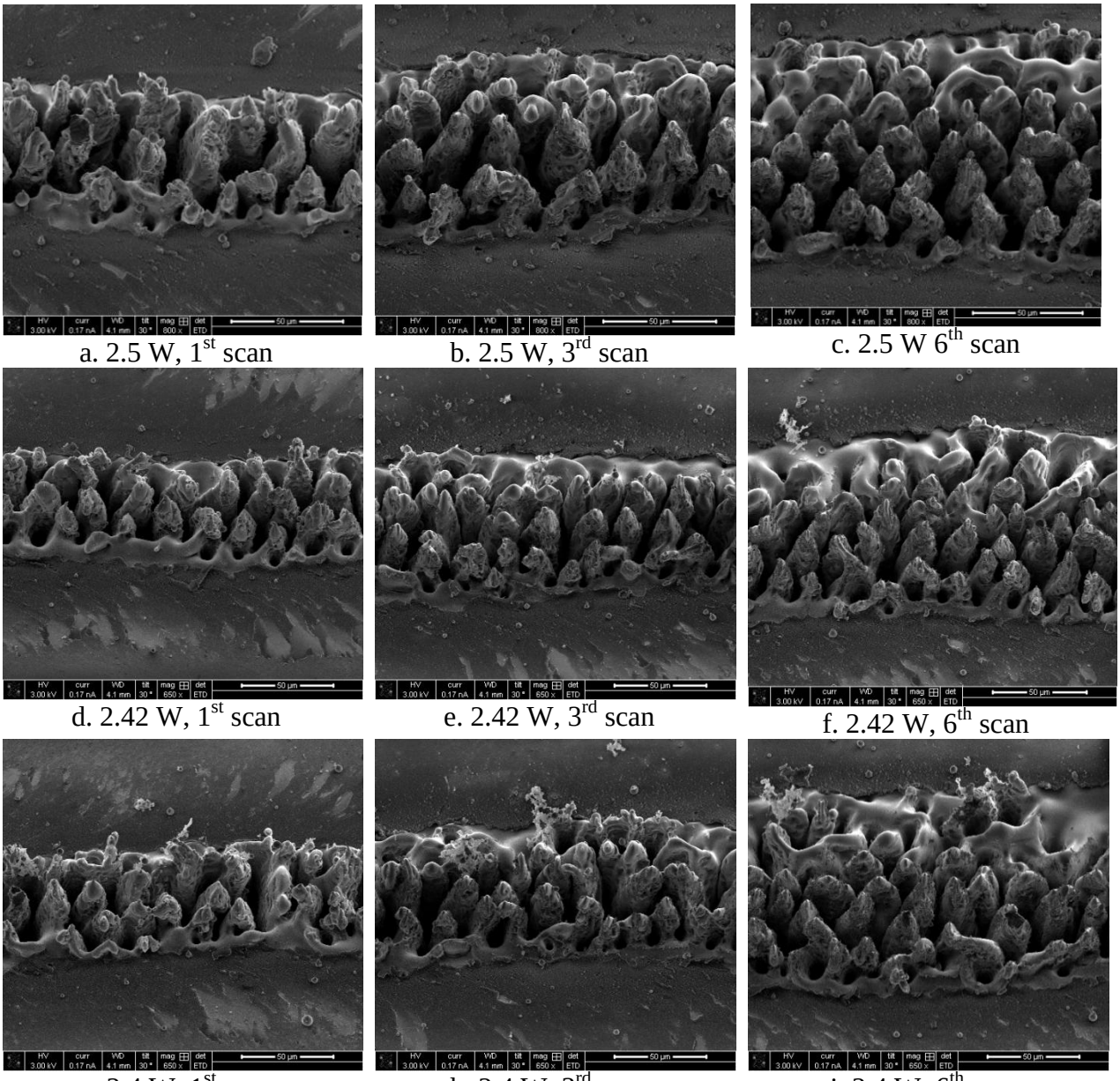

a. 2.5 W, 1st scan b. 2.5 W, 3rd scan c. 2.5 W 6th scan

d. 2.42 W, 1st scan e. 2.42 W, 3rd scan f. 2.42 W, 6th scan

g. 2.4 W, 1st scan h. 2.4 W, 3rd scan i. 2.4 W, 6th scan

Figure 4.13: Individual scanned lines at various power levels with a line spacing of 10 μm, a scanning speed of 10 mm/s and a pulse frequency of 10 kHz

Figures 4.13a, d, and g shows spikes after the scanning of just one line. There is clear evidence of ablation and surface melting across the structure. The size of the spikes seems to decrease as power is reduced. The 2.42 W case seems to have the structure with the highest degree of uniformity. This suggests that having too much power leads to ablation that decreases the quality of the structure, even after just one scan.

Figures 4.13b, e, and h shows that the uniformity of the structures improves along with marginal growth of the width compared to the previous textured areas. The spikes closer to the latest line scanned behaves as described in figures 4.13a, d and g. Additional pulses affect the higher surface area of the textured surface easier than the unprocessed area, which allows the

structure to be further modified.[3] The spikes in the processed area far away from the latest line processed are more uniform and more homogenous compared to the most recently created spikes. This could be a sign that multiple line scanning anneals the previously modified structure through the addition of a lower power level due to the characteristics of the beam's Gaussian profile. The annealing process may help to recrystallize the structure, reforming the loose structure, which would lead to a higher current density and device performance. This would remove an addition step of etching to remove the initially loose structure and defects, as found in several methods to effectively texture silicon.[3,50] A disadvantage of the etching process is that the longer it is used, the less rough the surface becomes. Another method used was to anneal the structure in flowing Ar, but this method decreases the below band-gap absorbance.[51] Both of the methods shown here require additional steps that would not be needed if the structure annealed during the processing.

Figures 4.13 c, f and i show a continual increase in the uniformity of the previously textured area. The 2.4 W case seems to be less uniform compared to the higher power cases. This suggests that there is not enough power in this case to completely anneal the structure at the same rate as the other cases.

In all cases except for the first scan lines for each power, there is a clear distinction between two layers in front of the latest scanned line. This could be evidence of the removal of the natural oxide layer before the high intensity of the center of the beam reaches the area. If this is accurate, the Gaussian beam profile could be used to pretreat the area just before it is processed.

4.4.3 Laser Parametric Study for Optimal Laser Texturing

A parametric study was conducted to determine the extent to which black silicon can be created. The parameters that were varied in this study include: laser power, line spacing, scanning speed and pulse frequency. The sample that was processed is shown below in figure 4.14:

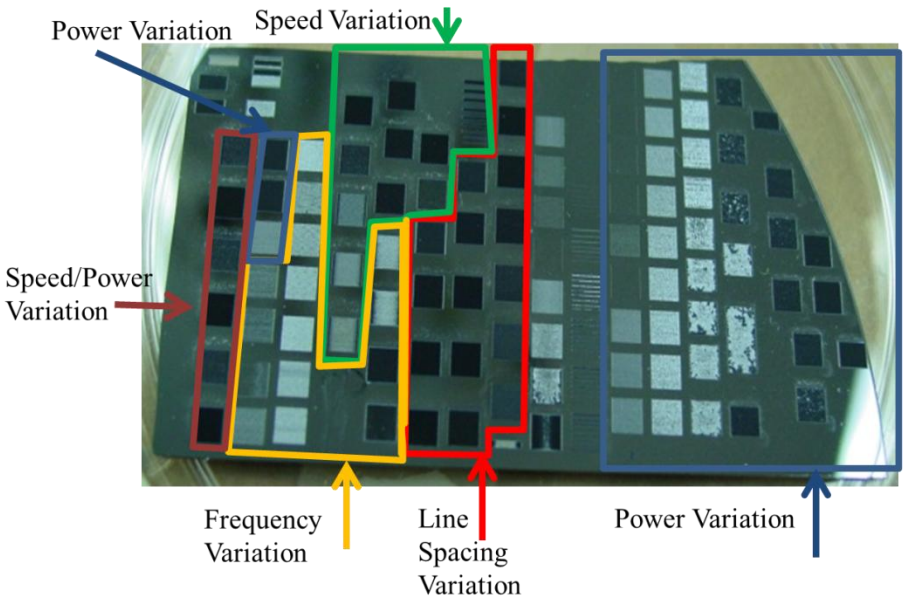

Figure 4.14: A parametric study conducted on a single silicon sample

Figure 4.14 shows that by visual inspection, black silicon was created under different conditions. Similar results were attained under different parameter selection.

4.4.3.1 Power Variation

For this part, the transition of the morphology of the silicon surface, as the power was varied, was desired. 41 squares were processed by varying the power of the laser between 1.08 W and 3.1 W. The line spacing of 10 μm, scanning speed of 10 mm/s, and a pulse frequency of 10 kHz were held constant. Each square took about 2 minutes and 21 seconds to process.

The specular reflection of nine points of interest was taken along with the reflection of the unprocessed area. These results are shown below in figure 4.15:

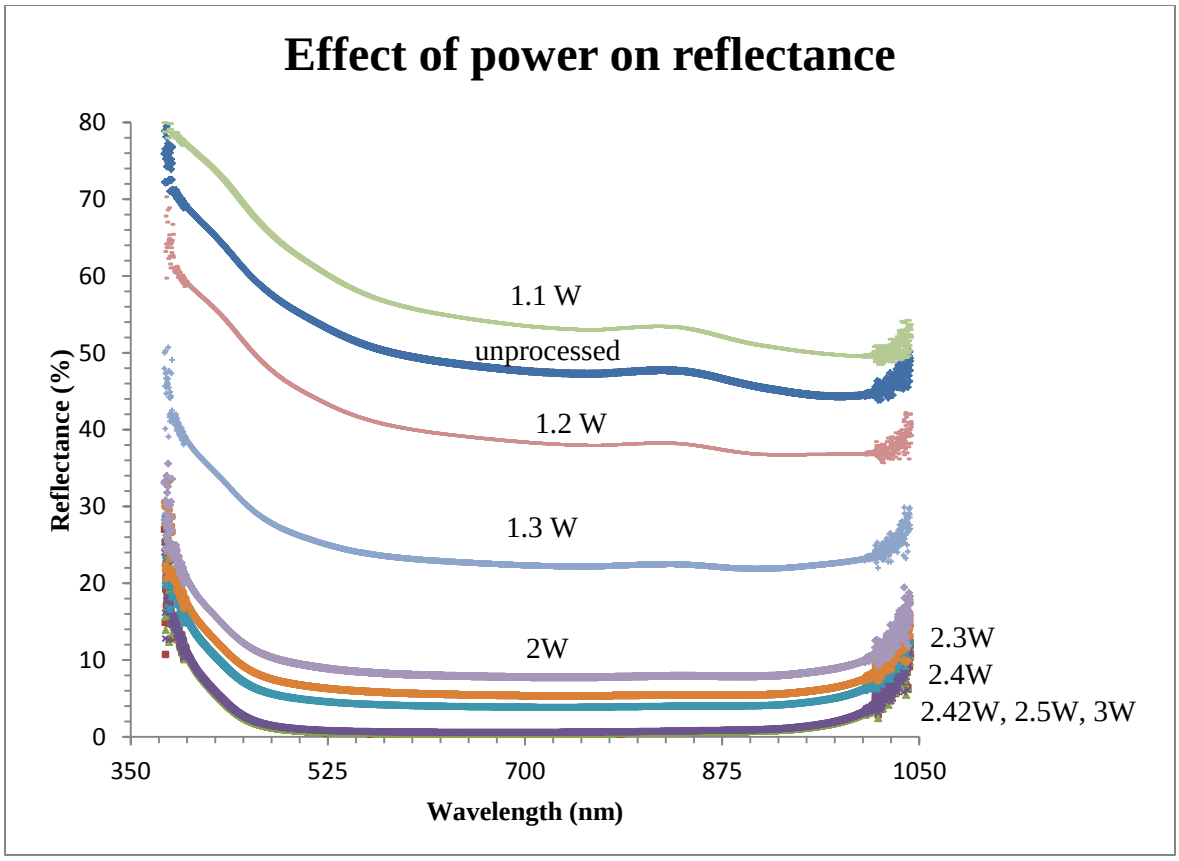

Figure 4.15: Specular reflection of silicon under various power levels with line spacing of 10 µm, scanning speed of 10 mm/s and pulse frequency of 10 kHz.

The overall trend is that specular reflection decreases as laser power is increases. The power levels leading to the lowest measured reflection varied from 2.42W to 3W. There is a relatively large decrease in reflectivity from 2.42W to 2.4W, signifying a transition. In order to gain an understanding of the mechanism that enabled this change, SEM images were taken of the various samples. Figure 4.16 shows SEM images of the points shown in figure 4.15:

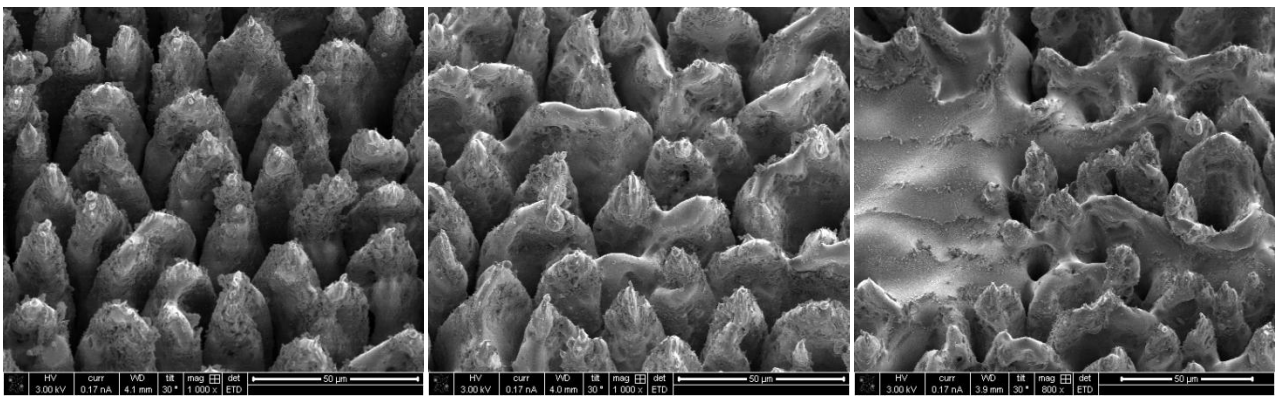

a. 3W b. 2.5W c. 2.42W

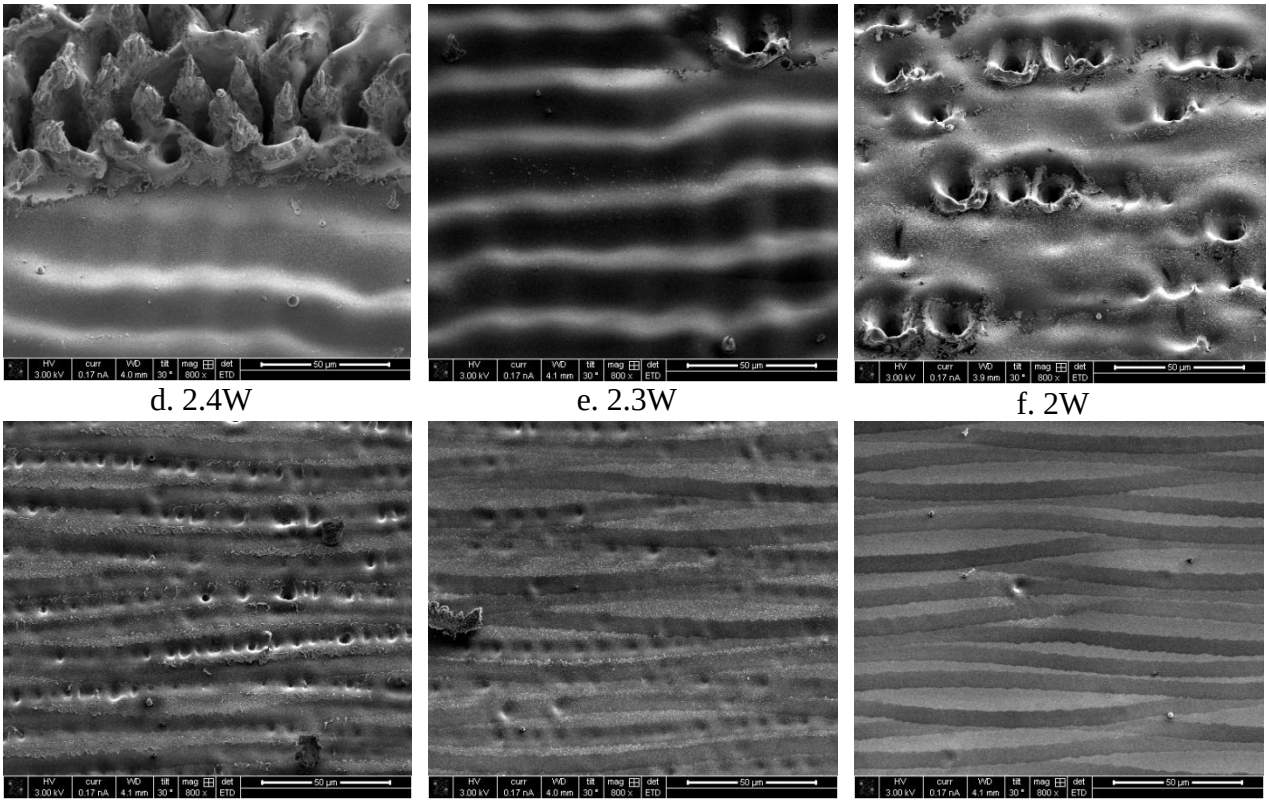

d. 2.4W e. 2.3W f. 2W

g. 1.3W h. 1.2W i. 1.1W

Figure 4.16: SEM images of silicon processing under various power levels with line spacing of 10 μm, scanning speed of 10 mm/s and pulse frequency of 10 kHz.

The structures of the 3W, 2.5W, and 2.42W cases are dominated by tall spikes and are visually seen as the color black. Figure 4.16c shows a lighter colored area in addition to the spikes. This seems to appear visually as the color silver. This processing area was not completely homogenous. There seems to be a great difference in surface structure and reflectivity between 2.42W and 2.4W. SEM pictures were taken several cases, on a larger scale relative to figure 4.16, in order to see the homogeneity of the structures, as seen below in figure 4.17.

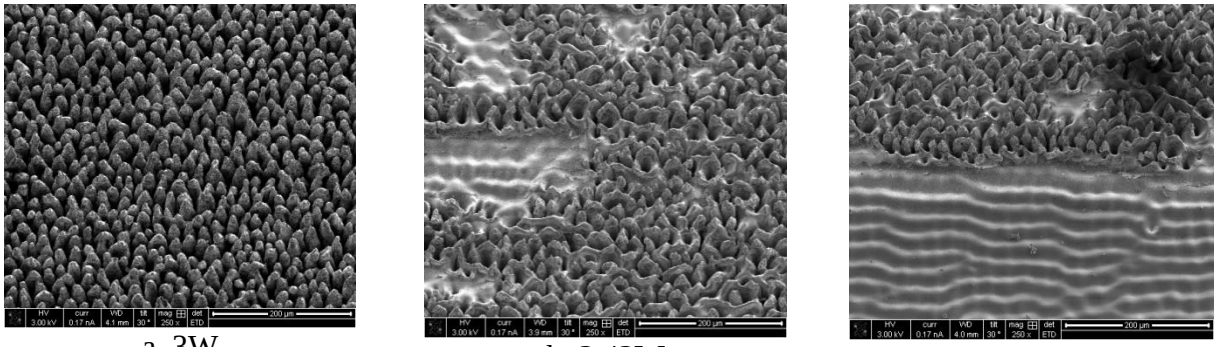

a. 3W b. 2.42W c. 2.4W

Figure 4.17: Large scale silicon processing under various power levels with line spacing of 10 μm, scanning speed of 10 mm/s and pulse frequency of 10 kHz.

Figure 4.17a shows a high degree of homogeneity. These results show an improvement over other methods of creating black silicon, which focus on growing the surface texturing from

the center.[6,7] Scanning at constant velocity allows for structural homogeneity to be attained.[4] The part of the structure that seems to be portrayed the color silver is the minority of figure 4.17b and becomes equal to the spiked structure in figure 4.17c. As an effect of this morphology change, the reflection of the silicon is higher for the 2.4W case along with a decrease in ablation.

By the time the laser power has been reduced to 2.3W, the surface appears to be completely silver, and the homogeneity of the structure returns. This suggests that a gradual transition occurs as the surface color changes from black to silver. For 2.0W, there is still some ablation, but the power has been decreased to a point where the surface cannot melt fully to improve the homogeneity of the structure. There is evidence of small ablation areas as power decreases until 1.2W, but as the power decreases, the affected area decreases as well.

The color appears to be shades of silver from 2.3W down until 1.3W. Below this point, the color seems to be similar to the unprocessed silicon. From 1.3W to 1.1W, the individual scanned lines can be seen.

4.4.3.2 Line Spacing Variation

Clearly, a decrease in the number of lines scanned would decrease the amount of time needed to complete a process. This section focuses on taking a single point that had achieved black silicon from section 4.4.3.1 and observing the effect of varying the line spacing. Squares were processed with line spacing between 10 μm and 100 μm. The power was set to 3 W, the speed was set to 10 mm/s, and the pulse frequency was set to 10 kHz.

The specular reflection of nine points of interest was taken. These results are shown below in figure 4.18:

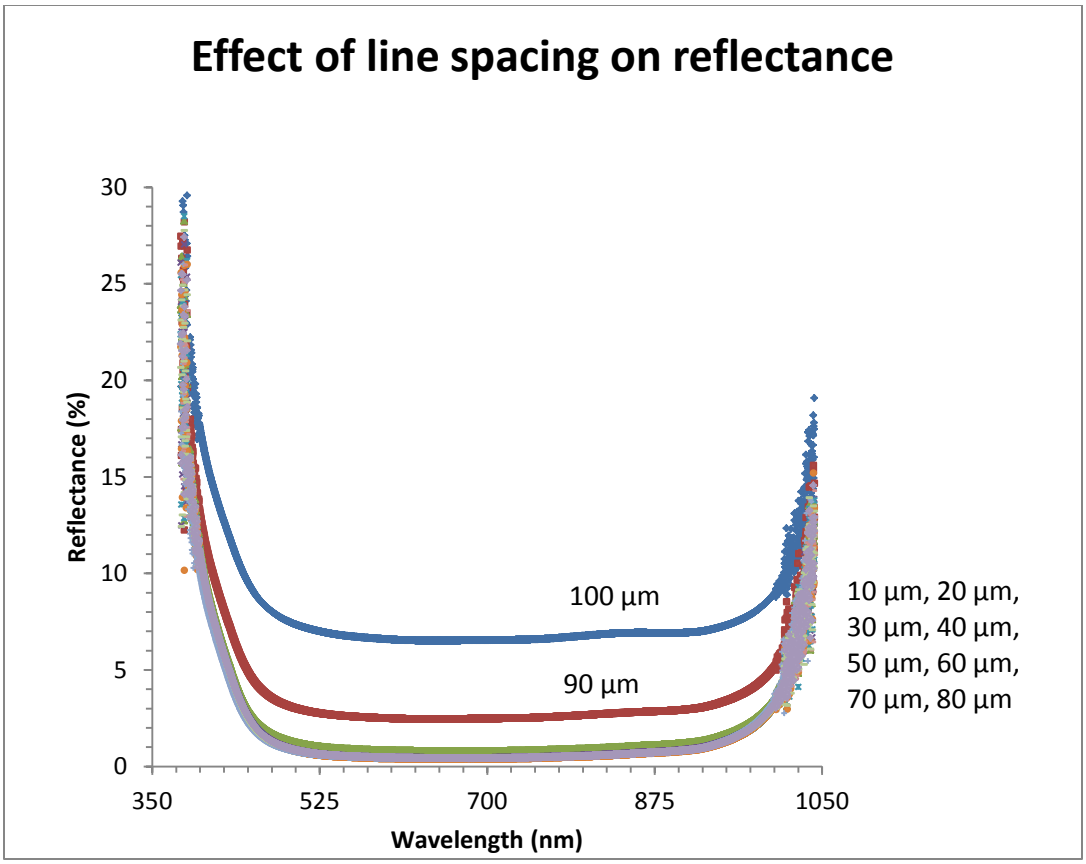

Figure 4.18: Specular reflection of silicon under various line spacing with laser power of 3 W, scanning speed of 10 mm/s, and pulse frequency of 10 kHz.

As the line spacing moves from 100 µm to 80 µm, the reflection decreases. The values from line spaces between 10 µm and 80 µm are close enough such that the effect of changing the line spacing cannot be determined. To resolve this issue, data for reflection was taken at 665.18 nm for all 10 processed areas, and plotted versus line spacing, as shown below in figure 4.19:

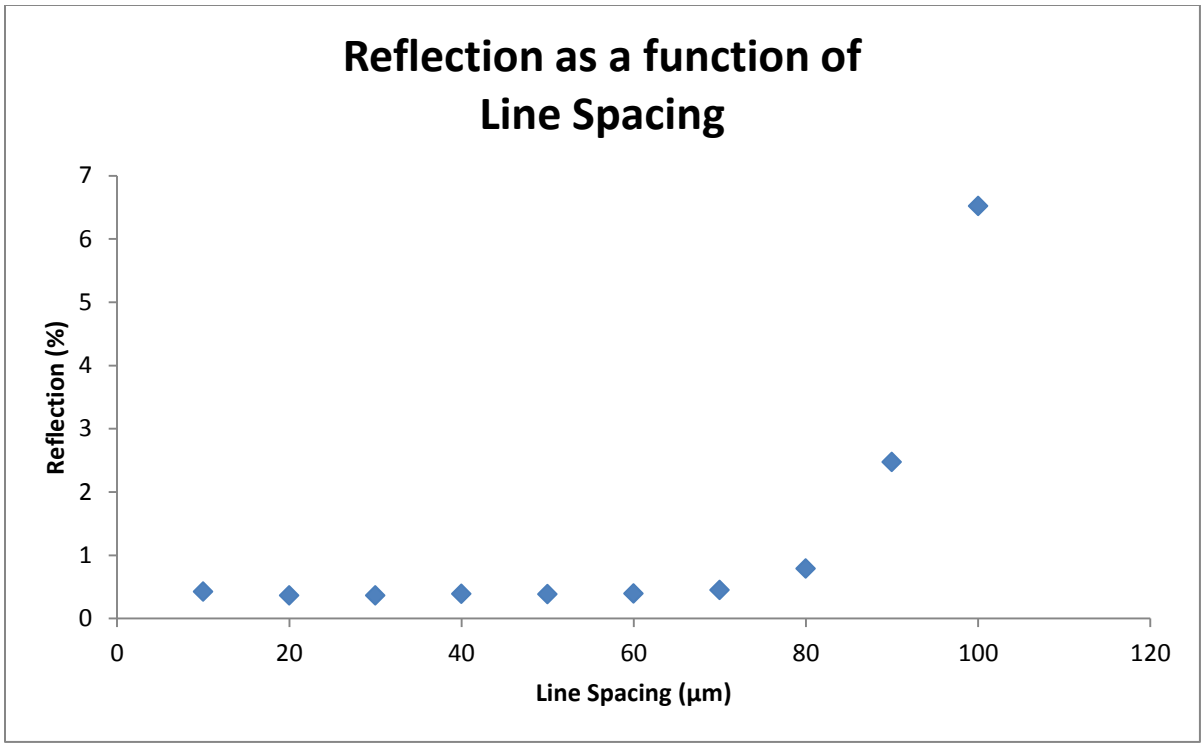

Figure 4.19: Specular reflection as a function of line spacing at a given point with pulse power of 3 W, scanning speed of 10 mm/s and pulse frequency of 10 kHz

The figure above shows that the specular reflection stays relatively constant at a line spacing at or below 70 µm.

To understand why this shift occurred, SEM images were taken for these areas. These results are shown below in figure 4.20:

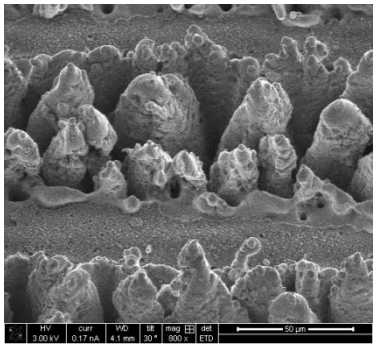

a. 100 microns

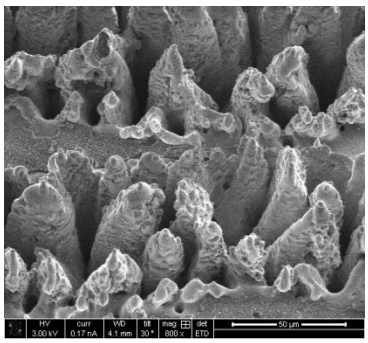

b. 90 microns

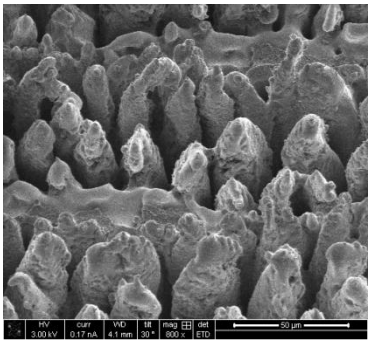

c. 80 microns

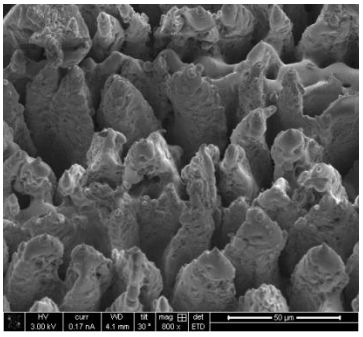

d. 70 microns

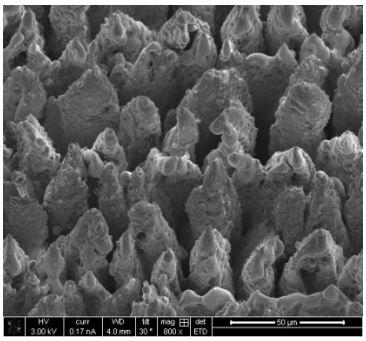

e. 60 microns

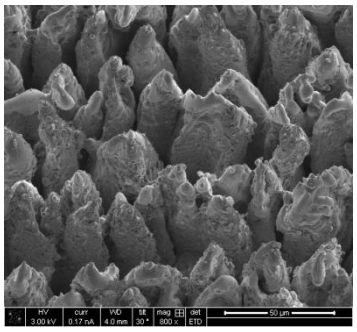

f. 50 microns

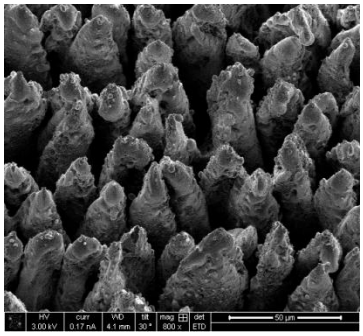

g. 40 microns

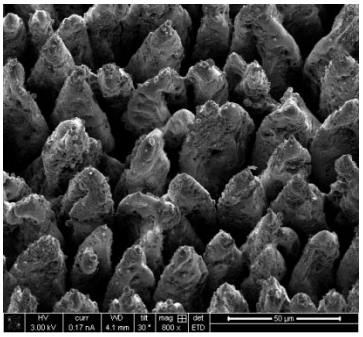

h. 30 microns

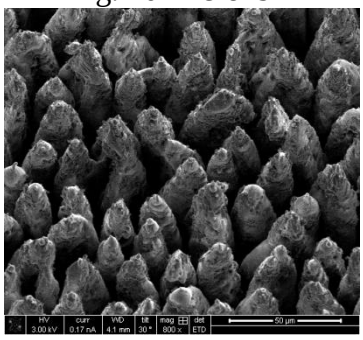

i. 20 microns

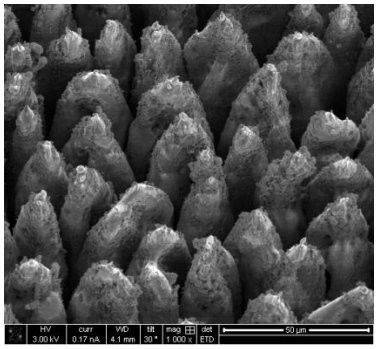

j. 10 microns

Figure 4.20:SEM images of silicon processing under various line spacing with pulse power of 3 W, scanning speed of 10 mm/s and pulse frequency of 10 kHz.

Figure 4.19 showed relatively high specular reflection levels for line spaces of 80 μm, 90 μm, and 100 μm. The SEM images from figure 4.20 support these results. Figures 4.18a, b, and c show regions that appear flat and unprocessed. These regions would reflect the light and increase

the overall reflectance. This has been reported for widely spaced ablated pits,[50] but can be adapted to scanning as well. The 100 μm spacing case had more regions like this compared to the 80 μm case, which would increase its reflectance. Since the 80 μm case did not have many of these regions, its reflectance is close to the other processed areas.

Even though the specular reflection seemed constant between the ranges of 10 μm and 70 μm, the SEM images do not look the same. The areas between 50 μm and 70 μm seem to have spikes melted together. On the other hand, the areas between 10 μm and 40 μm seem to have been annealed, and have a larger degree of homogeneity. As line spacing is increased, there becomes a point in which the Gaussian beam can no longer anneal the structure on subsequent passes. For this study, that threshold seems to lie between 40 μm and 50 μm. Yet, the specular reflection of all 7 cases is constant. This suggests that diffusive scattering plays a larger role for the processed areas with a line spacing between 50 μm and 70 μm.

4.4.3.3 Scanning Speed Variation

Scanning speed is an important parameter in determining effect of laser processing on materials, especially for industrial applications. Too slow of a scanning speed would take too long to process and may supply more energy than needed. A scanning speed too fast would not supply enough energy.

This section is broken down into two parts. For the first part, 8 areas were processed under the same conditions except for scanning speed. The laser power was set to 3 W, the line spacing was set to 50 μm, and the pulse frequency was set to 10 kHz. The scanning speed was varied from 1 mm/s to 50 mm/s.

The specular reflection of eight points of interest was taken. These results are shown below in figure 4.21:

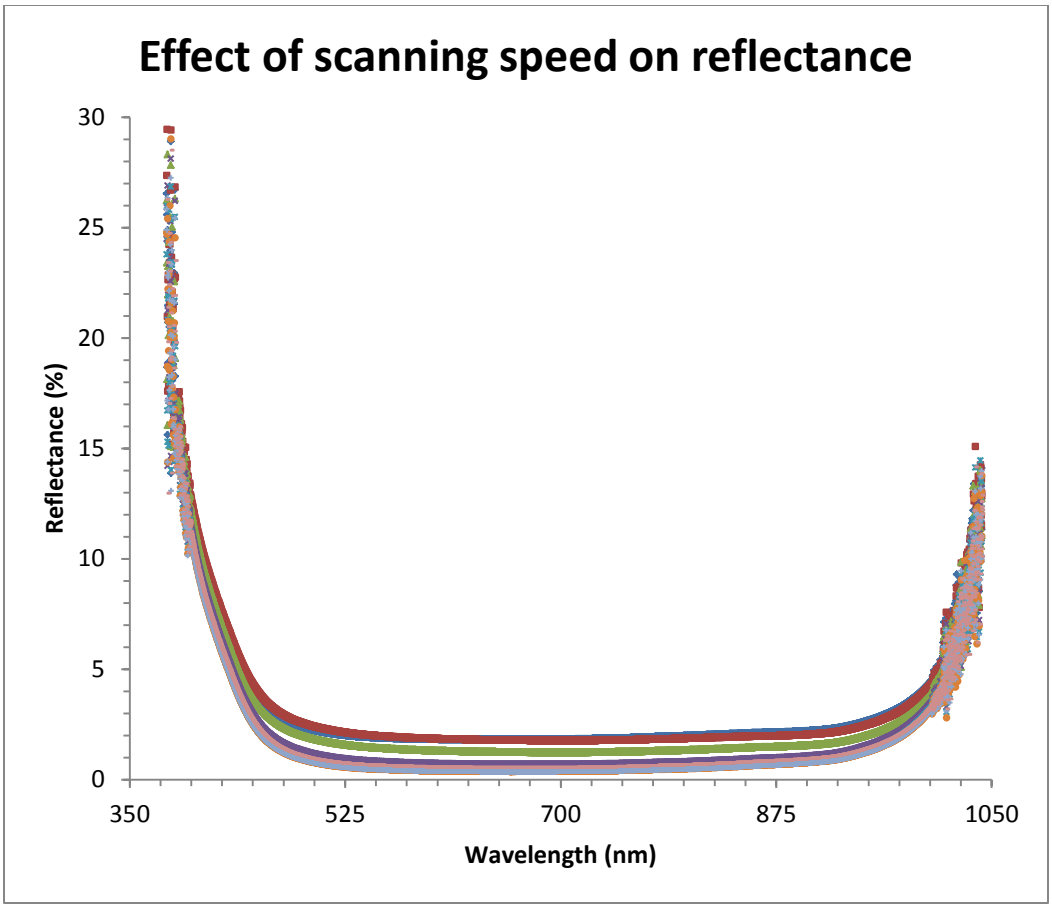

Figure 4.21: Specular reflection of silicon under various scanning speeds with constant: laser power of 3 W, line spacing of 50 μm and pulse frequency of 10 kHz

The lines are close enough that it is difficult to determine the reflection for any given scanning speed. To resolve this issue, data for reflection was taken at 653.96 nm for all 8 processed areas, and plotted versus scanning speed as shown below in figure 4.22:

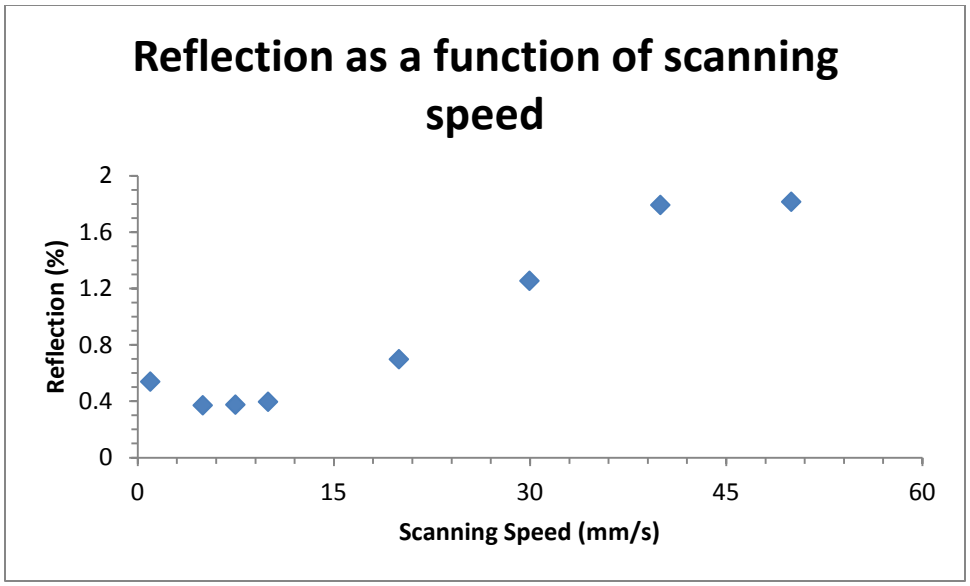

Figure 4.22: Specular reflection as a function of scanning speed with constant laser power at 3 W, line spacing at 50 μm, and a pulse frequency of 10 kHz

The figure above shows that the specular reflection stays relatively constant at its minimum between 5 mm/s and 10 mm/s. As the scanning speed increases, the reflection increases as well. This would be expected as there is not enough power to texture the surface.

SEM images were taken for these areas and the results are shown below in figure 4.23:

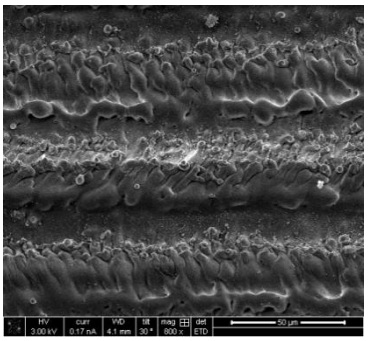

a. 50 mm/s

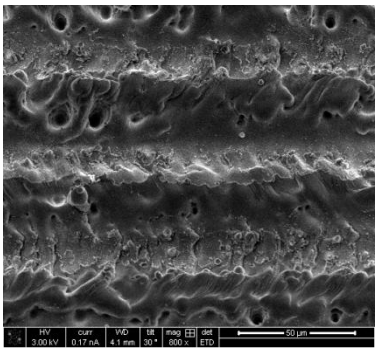

b. 40 mm/s

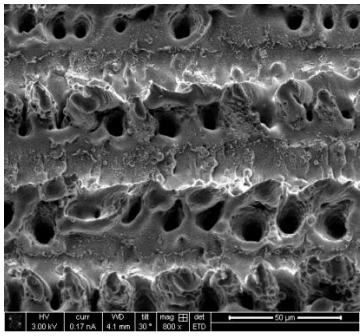

c. 30 mm/s

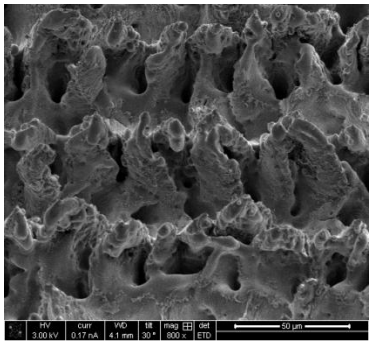

d. 20 mm/s

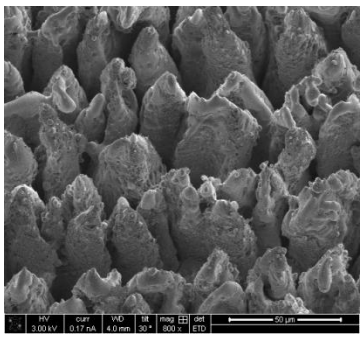

e. 10 mm/s

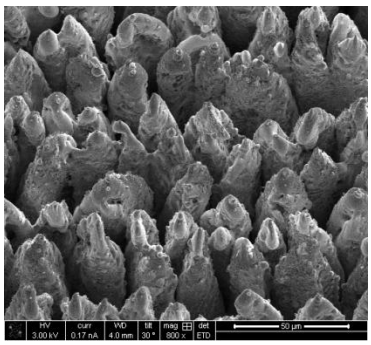

f. 7.5 mm/s

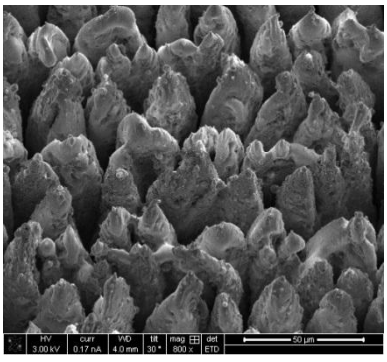

g. 5 mm/s

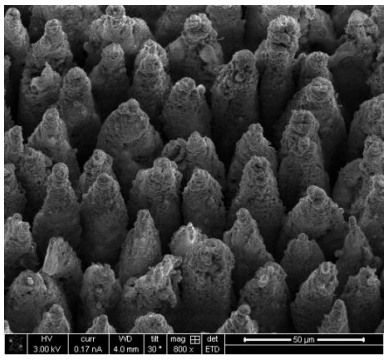

h. 1 mm/s

Figure 4.23: SEM images of silicon processing under various scanning speeds with constant: laser power of 3 W, line spacing of 50 μm and pulse frequency of 10 kHz

There exists a tradeoff between processing time and the quality of the textured surfaces.[7] The SEM images from figure 4.21 show three different kinds of structures. Figure 4.23a and figure 4.23b show clear periodicity in the y direction dictated by the line spacing of 50 μm. A

small amount of ablation seems to accumulate in the direction of scanning. There is also inhomogeneous melting of the structure. Figures 4.23c and d show the beginning of spike formation but there is still inhomogeneous structure and sporadic melting morphology. Figures 4.23e-h all shows well-formed spikes. The homogeneity improves as scanning speed decreases. In fact, it is surprising that the specular reflection for the 1mm/s case was higher than the other three considering its SEM image looks to be of higher quality of uniformity and homogeneity.

Since the scanning speed directly affects the amount of power needed for surface texturing, the experiment was repeated again with slightly different conditions. This time scanning speeds of 10 mm/s and 20 mm/s were used for four power levels between 2.5 W and 3 W.

The specular reflection of eight points of interest was taken. These results are shown below in figure 4.24:

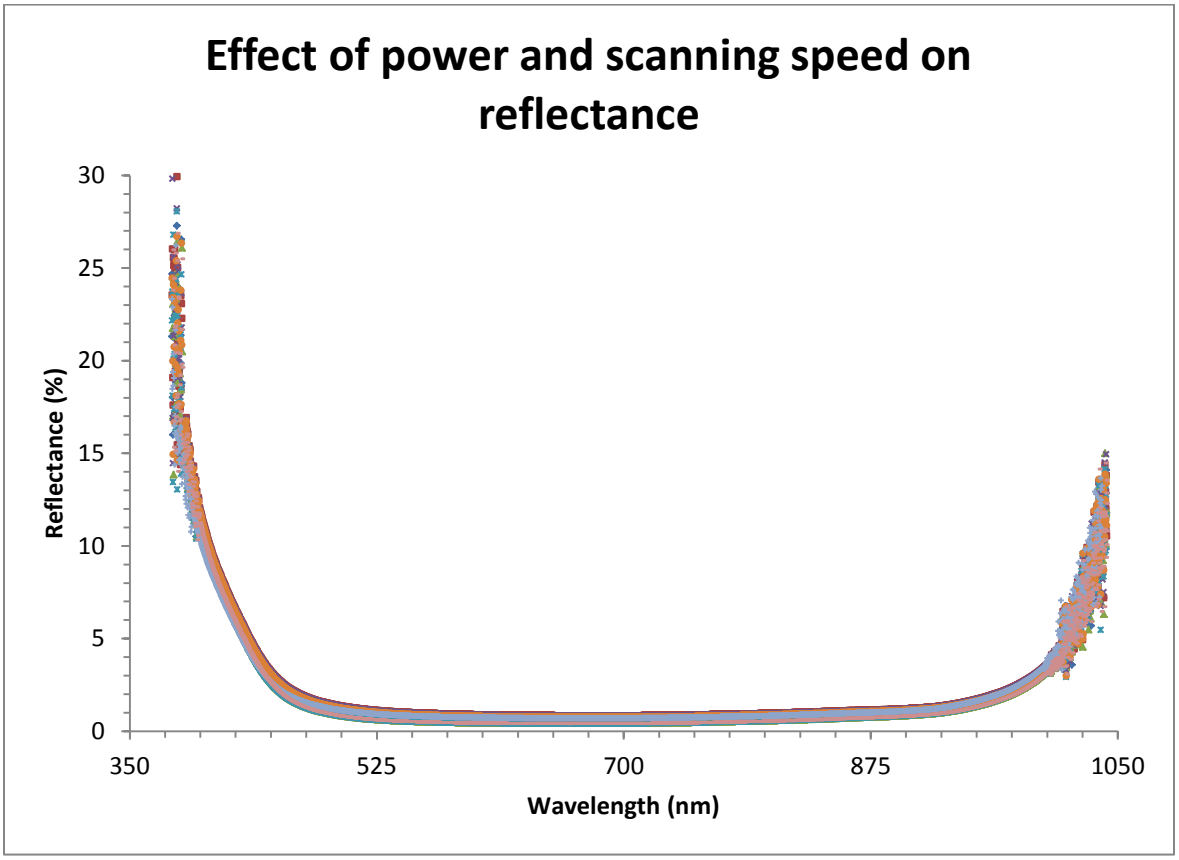

Figure 4.24: Specular reflection of silicon under various power and scanning speeds with constant line spacing of 50 μm and pulse frequency of 10 kHz.

The lines are close enough that it is difficult to determine the reflections for any given laser power and scanning speed. To resolve this issue, data for reflection was taken at 648.24 nm for all 8 processed areas, and plotted versus power as shown below in figure 4.25:

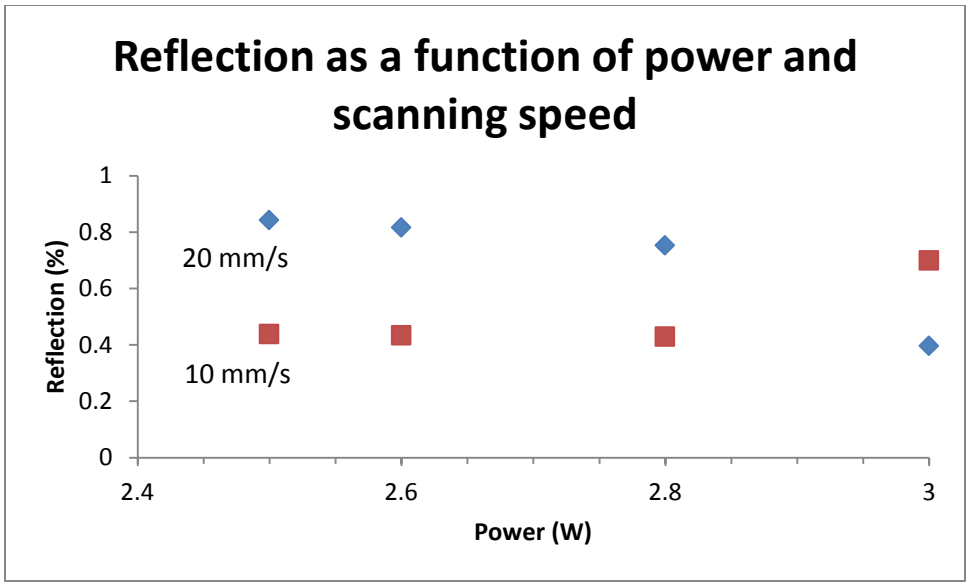

Figure 4.25: Specular reflection as a function of scanning speed under various power and scanning speeds with constant line spacing of 50 μm and pulse frequency of 10 kHz

Figure 4.25 shows constant results for both scanning speeds between 2.5 W and 2.8 W. The 10 mm/s cases achieve lower reflections, which would be expected if the power were not large enough to create a black surface for 20 mm/s cases. However, there is a shift at 3 W where the 20 mm/s case portrays a lower reflection than the 10 mm/s case. This tells us that at 3 W, there is enough energy being delivered to the surface to warrant an increase of scanning speed. SEM images were taken to confirm these results and can be found below in figure 4.26:

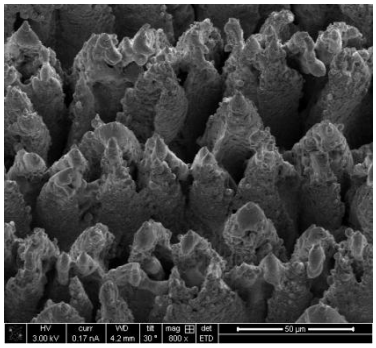

a. 2.5 W, 10 mm/s

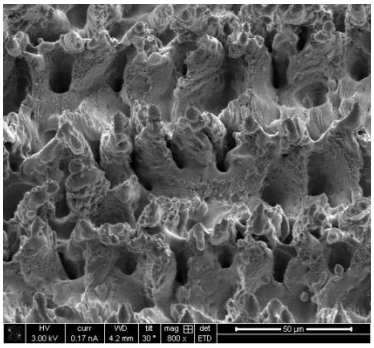

b. 2.5 W, 20 mm/s

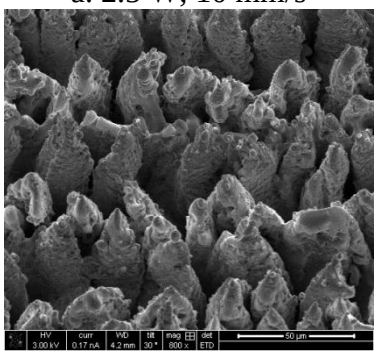

c. 2.6 W, 10 mm/s

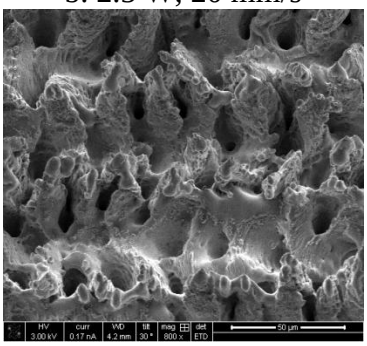

d. 2.6 W, 20 mm/s

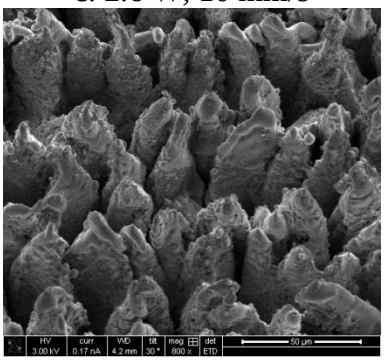

e. 2.8 W, 10 mm/s

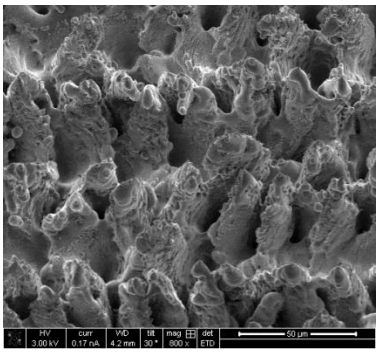

f. 2.8 W, 20 mm/s

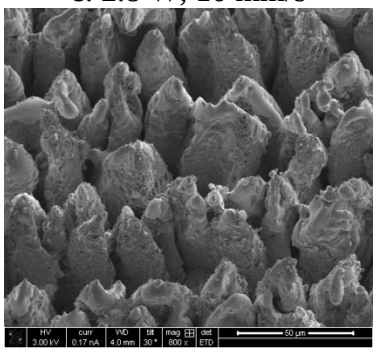

g. 3 W, 10 mm/s

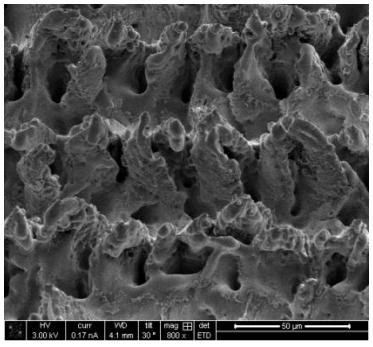

h. 3 W, 20 mm/s

Figure 4.26: SEM images of silicon processing under various powers and scanning speeds with constant line spacing of 50 μm and pulse frequency of 10 kHz

A scanning speed of 10 mm/s shows more homogeneity, less directional dependence and more controlled melting when compared to the 20 mm/s cases. With this in mind, it seems that

the reflection results do not agree with the SEM image for the 3 W, 20 mm/s case. As more energy is given to the processing area, a greater speed is desired to attain similar results.

4.4.3.4 Frequency Variation

Manufacturing plants in industry will have access to industrial lasers and scanning systems exceeding the capabilities of the equipment used in this research. A frequency variation was done to determine under what conditions black silicon could be created. Here, the line spacing was held constant at 10 μm. The other parameters varied depending on frequency.

The specular reflection of 3 frequencies of interest was taken. If the frequency is doubled, then the power and speed of the scanning should be doubled as well in order for similar results to be attained. These results are shown below in figure 4.27:

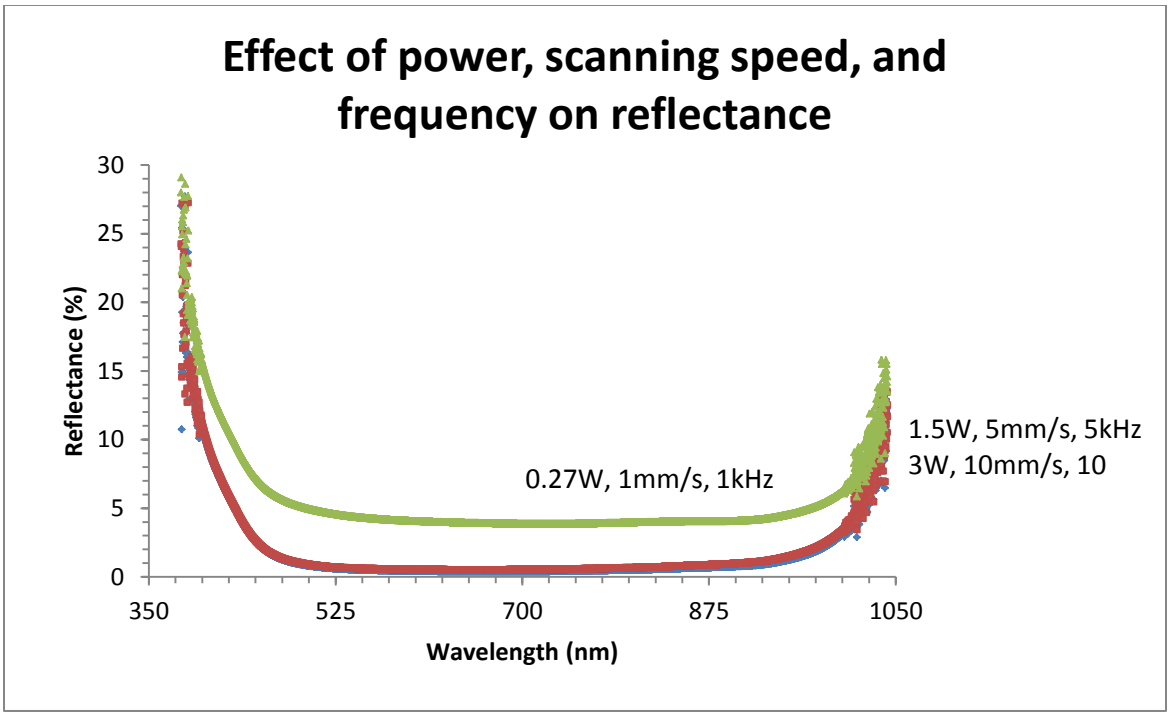

Figure 4.27: Specular reflection of silicon under various frequencies with line spacing held constant at 10 μm

As expected, the specular reflection of the 5 kHz and the 10 kHz cases are the same within error. The 1 kHz case has a much higher reflection. This suggests that there is a lower limit to the extent in which the relationship between laser power, scanning speed, and pulse frequency can be used.

SEM images of these three areas were taken and can be found below in figure 4.28:

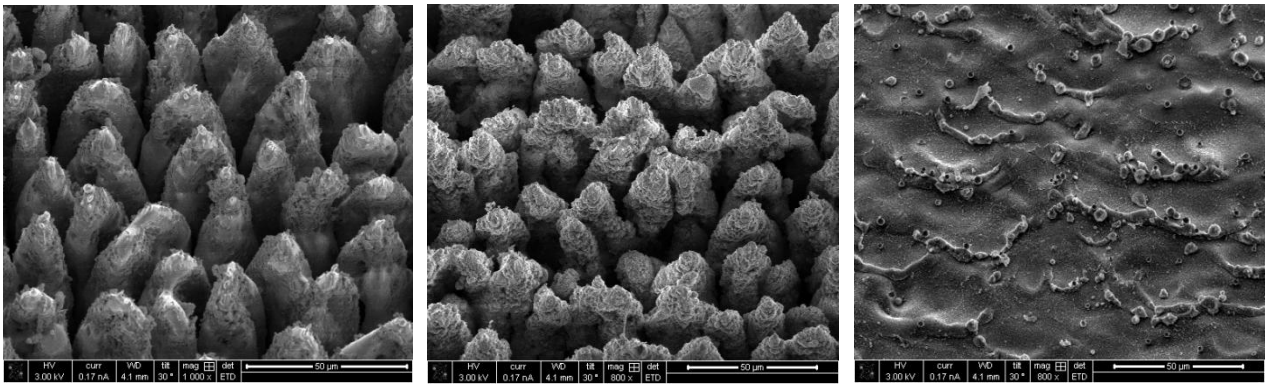

a. 10kHz, 10mm/s, 3W b. 5kHz, 5mm/s, 1.5W c. 1kHz, 1mm/s, 0.27W

Figure 4.28: SEM images of silicon processing under various pulse frequencies with constant line spacing of 10 μm

The SEM images show clear spikes for the 10 kHz and 5 kHz cases. The 10 kHz case seems to have more uniform structures in height, composition and distribution. On the other hand, the 1 kHz case does not show any spikes. Instead there is evidence of minimal melting and surface morphology modifications. This shows that there is a lower limit in assuming the relationship between parameters that is appropriate for the 5 kHz and 10 kHz cases.

Another test was done using a pulse frequency of 20 kHz. At that frequency, the maximum laser power was 2.75 W. To make the color of the silicon black, the expected power at this frequency is 6W. Since that was not possible, the area was processed with a pulse frequency of 20 kHz, along with a scanning speed of 20 mm/s and a laser power of 2.75 W. This condition was compared to an area processed with a pulse frequency of 10 kHz, a scanning speed of 10 mm/s, and a laser power of 1.35 W. The specular reflections of these two cases along with their SEM images are shown below in figure 4.29 and figure 4.30 respectively:

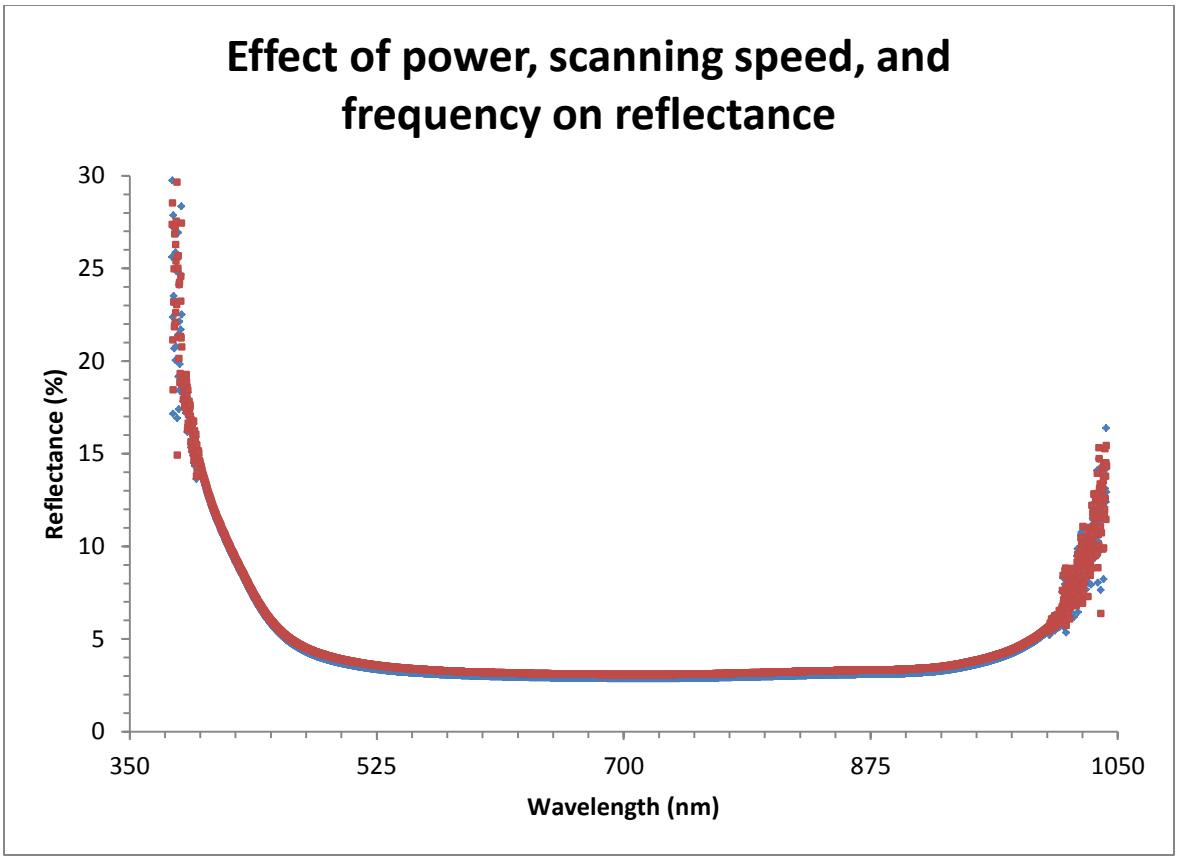

Figure 4.29: Specular reflections of silicon under two frequency cases. The first case is 1.35 W, 50 µm, 10 mm/s, and 10 kHz. The second case is 2.7 W, 50 µm, 20 mm/s, and 20 kHz

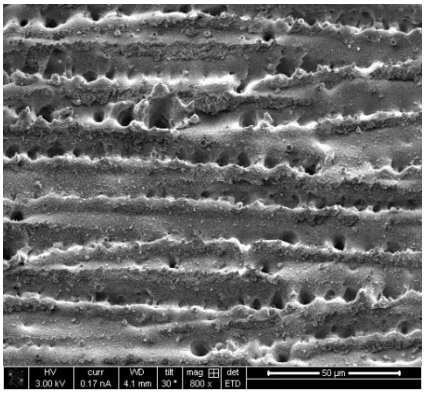

a. 10kHz, 10mm/s, 1.35W

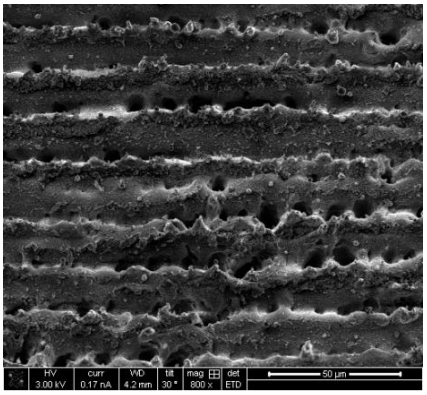

b. 20 kHz, 20mm/s, 2.7W

Figure 4.30: SEM images of silicon processing under two frequency cases

The specular reflections of the two cases in figure 4.29 looks the same. This can also be said about the general morphology of the SEM images. This shows that the relationship between laser power, scanning speed and pulse frequency that determines the color and structure of silicon can be transformed to different frequencies from 5 kHz to 20 kHz. Frequencies beyond 20 kHz may be valid as well, but have not been tested up to this point.

4.4.4 Effect of Laser Scanning Speed towards Practical Processing Speed

All of the prior subsections have been about scanning the laser beam back and forth to achieve the desired results. Here, the focus will be on determining the effects of a single pulse. To do this, the scanning speed was set to the maximum speed for the motion stage (400 mm/s). The pulse frequency was set to 10 kHz. A single line with a length of 1.5 cm was scanned for a variety of power levels between 3 W and 1.1 W. The theoretical distance between pulses from equation 4.3 is again utilized. This time the parameters are a scanning speed at 400 mm/s and a pulse frequency at 10 kHz. Equation 4.1 predicts the distance between pulses to be 40 μm.

SEM images are shown below in figure 4.31:

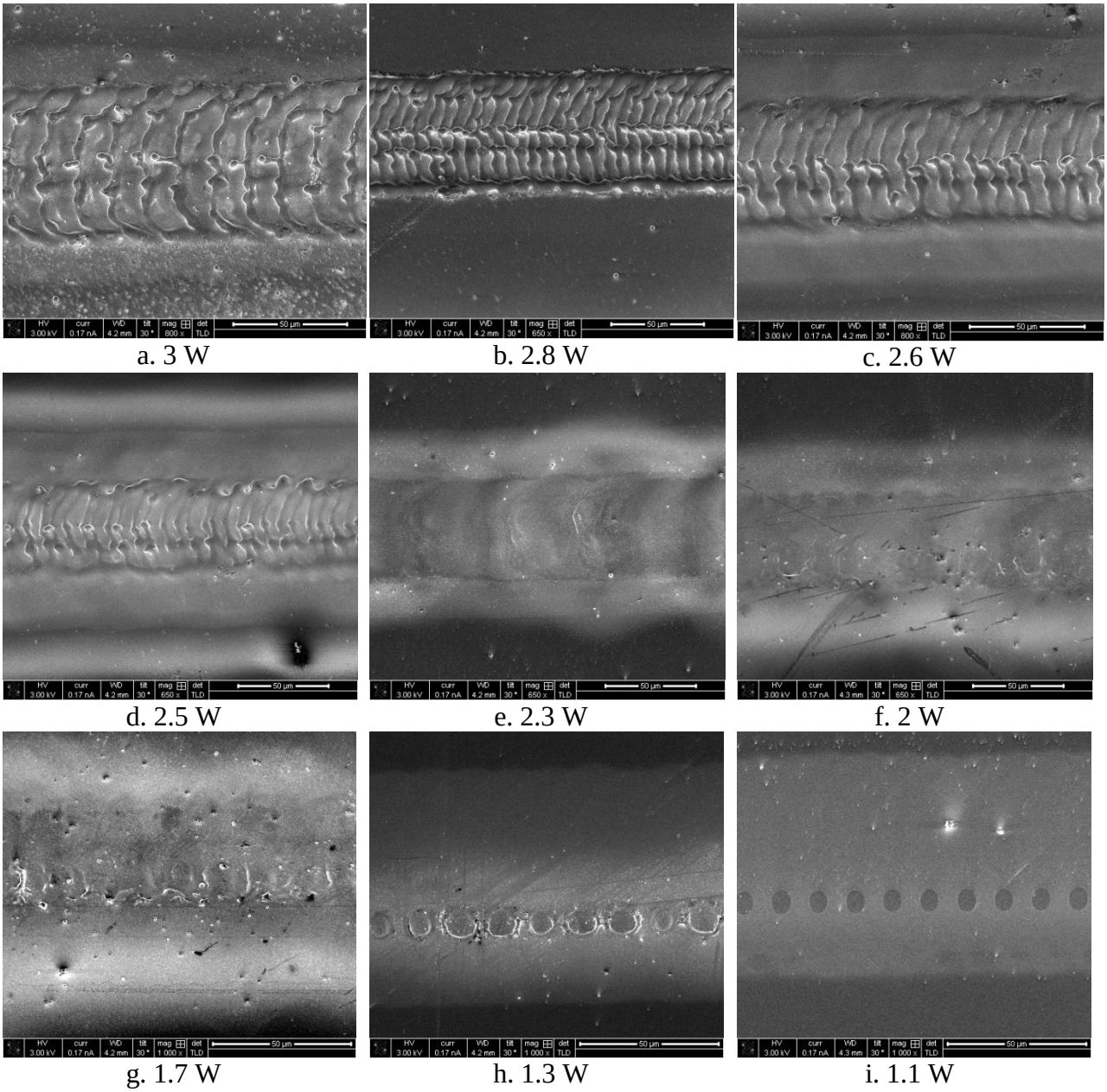

a. 3 W b. 2.8 W c. 2.6 W

d. 2.5 W e. 2.3 W f. 2 W

g. 1.7 W h. 1.3 W i. 1.1 W

Figure 4.31: SEM images of a single scan at various power levels

For all of the cases in figure 4.31, there is some degree of melting. From figure 4.31a through figure 4.31d, periodic structures form along the scanning direction with an approximate spacing of about 5 μm. The shape of the structures suggests that there are interactions between adjacent pulses coupled with capillary motion.

From figure 4.31e through figure 4.31g, there is still surface melting and the path of the laser beam can clearly be seen. The morphology change seems to be less than the prior cases. This would be expected for a reduction of power. For figure 4.31f and figure 4.31g, the energy irradiated onto the surface is not large enough to change the surface defects that are present on the surface.

Individual pulses can finally be seen for figure 4.31h and figure 4.31i. The 1.3 W case shows bumps around the outside of each pulse, which are absent for the 1.1 W case. The pulse spacing, as seen from figure 4.31i, is approximately 10 μm, four times shorter than the theoretical value. There are two possible explanations for this discrepancy. It is possible that the laser did not scan far enough for the true steady state speed of 400 mm/s to be achieved. The second possibility is that there was some marginal error in the Nd:YAG laser such that the actual frequency is not quite 10 kHz. Regardless, it was found that a single pulse was able to modify the surface even on the lowest power setting.

4.5 Summary of Laser based Texturing of Silicon

Black silicon was created by rapid laser surface texturing. The processing produced a high degree of uniformity over an arbitrary surface area. The surface structure evolves based on laser ablation and melt induced capillary flow. Annealing of the structure comes from reheating of the previously textured surface to improve the carrier transport. A parametric study was conducted by varying process parameters to show that broad processing range enabled optimization of the process in terms of process quality, process size, and processing time. The effect of scanning speeds towards practical processing speeds was also analyzed and displays the requirement for higher pulse energy at higher speeds.

CHAPTER 5: FURTHER ENERGY APPLICATIONS BASED ON LASER-ASSISTED TEXTURING

The majority of the work presented here was designed for solar cell application. Rapid scanning laser processing can be applied to various fields. Enhancement of emissivity through surface texturing for applications such as heat exchangers will be shown in section 5.1. Section 5.2 will cover surface texturing for the anode and cathode of fuel cells. Section 5.3 will show surface texturing for biofuels. A brief summary of surface textured energy applications will be shown in section 5.4. For section 5.2 and section 5.3, the goal is to increase the surface area by roughening the surface through rapid scanning of a laser beam. Other notable applications of rapid scanning laser texturing can be applied to: batteries[52], adhesion of thermal sprayed thin film[53] and creating wetted surfaces.[54]

5.1 Surface Texturing to Enhance the Emissivity for Heat Exchanger Applications

As mentioned in previous sections, surface texturing of a material's surface induces structural and optical modifications. A notable modification from laser induced surface texturing is the change in the emissivity of the surface. Emissivity is defined as a measure of how close a surface is to a blackbody.[55] A black body absorbs all of the incident radiation and appears to have a black color.

A slab of aluminum was heated up using a lamp. This was done to elevate the temperature of the metal above the temperature of the room. Processed silicon and copper were placed on the aluminum and a picture of the temperature fields were taken using an IR camera. Pictures of the samples as well as an IR image of the sample are shown below in figure 5.1 and figure 5.2 for silicon and figure 5.3 and figure 5.4 for copper:

Figure 5.1: Picture of silicon

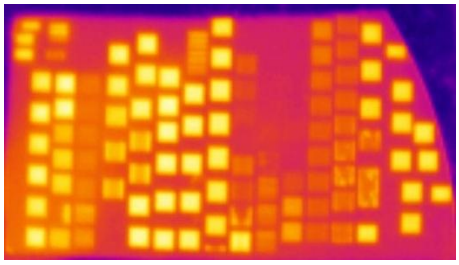

Figure 5.2: IR image of silicon

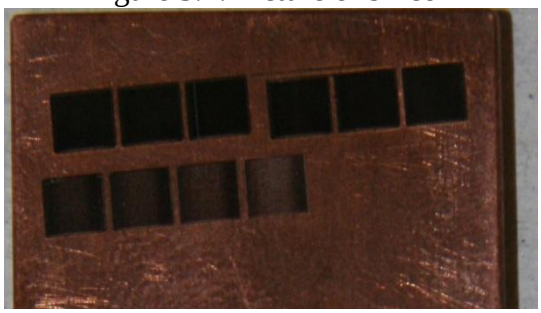

Figure 5.3: Picture of copper

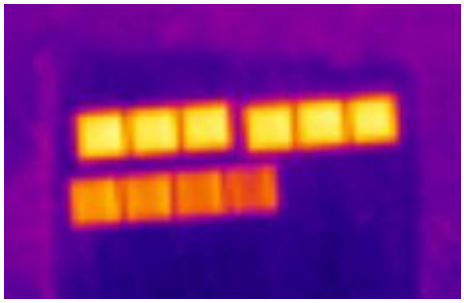

Figure 5.4: IR image of copper

The silicon was processed as described in section 4.3.3. The copper was processed on an earlier revision of the experimental setup which was not as precise, but sufficient for a preliminary study. For the copper, 3 mm by 3mm squares were processed with a line spacing of 10 μm, a scanning speed of 10 mm/s, a pulse frequency of 10 kHz, and a power variation between 3.46 in the upper right square and 1.6 in the lower left square. The supplied power was highest in the top left square and lowest in the bottom right square.

The aluminum plate is shown as blue in figure 5.2 and light purple in figure 5.4. The materials seem to be of a higher temperature. Since the silicon and copper were originally at room temperature and the only source of heat is the aluminum plate, the materials cannot be at a higher temperature then the plate. The brighter colors in figure 5.2 and figure 5.4 indicate an increase in emissivity. The areas in figure 5.1 and 5.3 that visually looks black, appear brighter in figure 5.2 and figure 5.4. This indicates that these processes have a higher relative emissivity, which would be expected for a black color.

It was shown that texturing the surface, shown visually by appearing black in color, increased the emissivity of the surface. Surfaces with high emissivity can be used as evacuated tube solar collectors and heat exchangers. Evacuated tube solar collectors used solar irradiation to heat water through a copper tube. The tube is placed in a transparent tube under vacuum to remove all heat losses due to conduction and convection. Texturing the surface of the copper tube with lasers would increase the emissivity, as shown in figure 5.4, improving the absorption of energy and the overall efficiency. Increasing the emissivity of heat exchangers through laser texturing would allow for heat to be radiated at a relatively higher rate.

5.2 Surface Texturing for Fuel Cell Application

Fuel cells are becoming increasingly notable as an alternative to the traditional batteries. Fuel cells operate by chemical reactions from hydrogen and oxygen producing electricity and water.[56] Varieties of fuel cells include: Akali, Molten Carbonate (MCFC), Phosphoric Acid (PAFC), and Proton Exchange Membrane (PEM). An example of PEM fuel cell is shown below in figure 5.5:

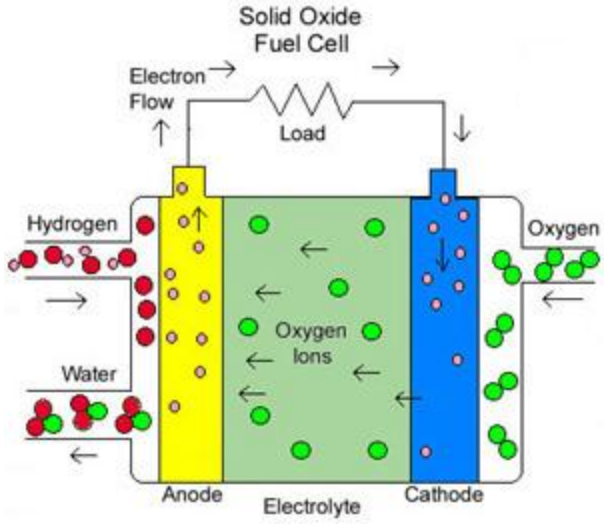

Figure 5.5: PEM Fuel Cell[54]

Hydrogen chemical reacts at the anode, providing electrons for the electrical circuit. The oxygen chemically reacts to the cathode, gaining electrons and becoming oxygen ions. The oxygen moves across the electrolyte and recombines with hydrogen at the anode, which creates water. The anode and the cathode are separated by an electrolyte that allows for oxygen ions to cross but prevents the flow of hydrogen and electrons. In this case the electrolyte is a solid, but is a liquid for other variants.

The biggest issue with mass producing fuel cells is the cost. Each variant of fuel cells uses its own set of materials for the anode, cathode, and electrolyte as well as conditions such as operating temperature. In each case, the cost of materials and manufacturing processes makes these cells expensive compared to other options.

Rapid scanning laser processing can be used to texture the surface of the anode and cathode of fuel cells. The increased surface area is proposed to lead to an enhancement of efficiency due to a relatively higher rate of chemical reactions. This hypothesis was tested by conducting electrolysis for unprocessed 304 stainless steel and processed 304 stainless steel. By measuring the relative production of hydrogen and oxygen, the relative efficiency can be attained. The following figures show the Hoffman apparatus, processed stainless steel before electrolysis, and processed stainless steel after electrolysis:

Figure 5.6: Hoffman Apparatus

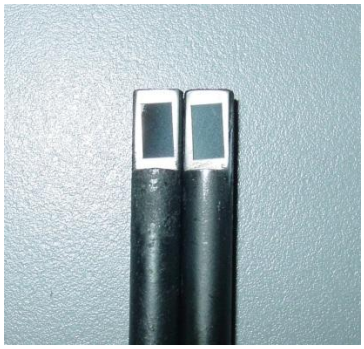

Figure 5.7: Processed Stainless Steel before Electrolysis

Figure 5.8: Processed Stainless Steel after Electrolysis

Each piece of stainless steel includes one end that was machined on both ends to make a flat surface for the processing. The rest of it is spray-painted black to prevent it from interfering in the measurements.

Figure 5.6 shows the unprocessed stainless steel in the Hoffman apparatus. The steel was placed in a solution of potassium hydroxide. A constant voltage of 4 V was applied. The same conditions and alignment was used for the processed stainless steel case. The table below shows the current produced as a function of time:

Table 5.1: Electrolysis current as a function of time

Time (min)	Current for Unprocessed Case (mA)	Current for Processed Case (mA)
0	80	23
1	65	8.5
2	57	4.7
3	45	4
4	40	3.7
5	38	3.9

The current produced for the processed case is drastically lower compared to the unprocessed case. This suggests that the hydrogen and oxygen produced should be higher for the unprocessed case. 1 cc of oxygen and 2 cc of hydrogen were produced for the unprocessed case and nothing was produced for the processed case. The laser scanning made the efficiency of electrolysis worse. The differences in figure 5.7 and figure 5.8 should be noted. After being placed in the potassium hydroxide, the paint corroded and there was significant change to only one of the processed steel pieces. This sample turned darker in the processed area and the unprocessed area turned blue. This suggests that the laser processing initiated a chemical change to the surface structure not only where the processing was visible but to the surrounding area as well. Currently, laser processing does not improve efficiency of the anode and cathode, but further tests need to be conducted to see the total effects of laser processing.

5.3 Surface Texturing for Biofuel Application

For biofuels, rapid scanning laser processing can be applied to the production of bio fuels, in particular, algae growth. Algae can be grown and extracted for oils, thus making it a renewable source of energy.[57] Laser texturing of stainless steel plates can be used to enhance the growth of algae, shown below in figure 5.9:

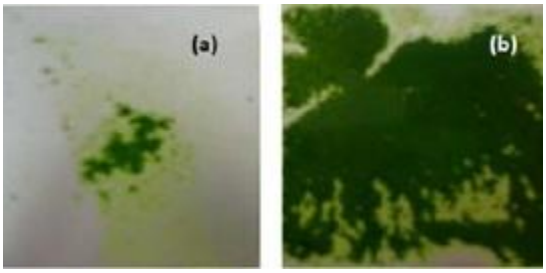

Figure 5.9: algae growth on: (a) unprocessed stainless steel and (B) laser textured stainless steel

The textured surface clearly enhances the growth of algae.

Rapid scanning laser processing was used on 304 stainless steel, producing 3mm by 3mm squares with line spacing of 10 μm, and a pulse frequency of 10 kHz. Power variation was done with a scanning speed of 10 mm/s for the top two lines and a scanning speed of 20 mm/s for the bottom line. For the 10 mm/s case, the power is highest at 3.25 W at the upper right most square and decreases to the left. The lowest power is at the left most square of the middle line with a power of 0.5 W. For the 20 mm/s case, the power is highest at the right with 3.05 W and lowest on the left with 1.7 W. The same setup as for the silicon in chapter 4 was used here. The sample is shown below in figure 5.10:

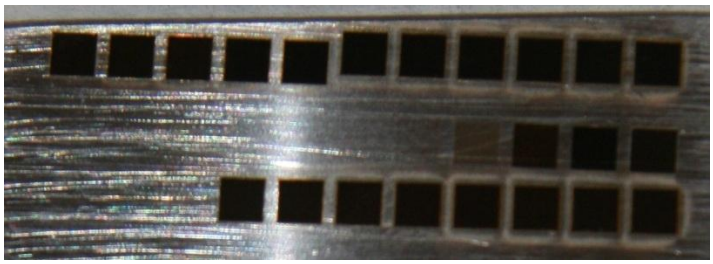

Figure 5.10: Processed stainless steel with 10 μm spacing, a pulse frequency of 10 kHz, and with variations of power and scanning speed

In the figure above, the surface color of stainless steel varied as power is decreased from black to brown, to several semi-transparent colors that do not fully appear in the figure. Algae growth has not yet been performed on these samples but is projected to enhance the growth depending on the degree of texturing. Rapid scanning laser processed can be used to texture an arbitrary surface quickly and efficiently.

5.4 Summary of Surface Textured Energy Applications

This chapter showed the results for surface texturing applications. Laser induced surface texturing were shown to enhanced emission for solar collectors and heat exchangers. Laser induced surface texturing produced poor results for the electrode of fuel cells, which has been

attributed to the high degree of ablation. Varied surface texturing of stainless steel was also produced to show application to algae growth.

CHAPTER 6: SUMMARY AND FURTHER STUDY

The focus of this thesis was on rapid laser scanning surface texturing of silicon for solar cell applications. In addition, there were some preliminary experiments performed on copper for solar collector and heat exchanger applications and stainless steel for biofuel and fuel cell applications. A summary of this work will be presented in section 5.1. Section 5.2 will describe ongoing experiments that will be performed to further support the results shown here.

6.1 Summary

Chapter two described the need of improving the utilization of renewable energy resource. This work was motivated by the desire to make renewable energy competitive against nonrenewable energy. Even though renewable energy production is currently relatively low, the potential is great. Solar energy by itself has the possibility to generate enough energy to power the country. Laser processing can make this technology a viable solution to the energy problem in this country.

Chapter three briefly explains laser processing, relevant heat transfer mechanisms, and the characterization methods of the laser-processed samples. The operation of lasers, and optical components was briefly described. Relevant heat transfer mechanisms were described to gain insight on laser-material interactions. These mechanisms include: ablation, surface melting, and capillary driven flow. Characterization techniques were described to analyze the samples. These techniques include: optical spectrometer, electron microscopy, focused ion beam, and the Hoffman apparatus.

Chapter four will focused on the silicon solar cell. Solar cell operation was explained and current advances in this field were briefly described. Black silicon was created by rapid laser scanning under various processing conditions. The surface structure evolves based on laser ablation and melt induced capillary flow. This process was able to achieve uniformity over an arbitrary surface area. Annealing of the structure comes from reheating of the previously textured surface. The annealing improves the carrier transport. A parametric study was conducted and show that broad processing range enabled optimization of the process in terms of process quality, process size, and processing time. The effect of scanning speeds towards practical processing speeds was also analyzed.

Chapter five described other energy related surface texturing applications to this process. Preliminary results were shown for surface texturing for applications such as: enhanced emission for solar collectors and heat exchangers, electrodes in batteries and fuel cells, algae growth and adhesion of thermal-sprayed thin films. Even though the results for laser texturing electrodes for fuel cells were poor, optimization and possible reduction of power to remove the dominate ablation regime can to the desired enhanced quality of fuel cells.

6.2 Further Study

The future study for this work can be broken down into four categories: improving processing speed, further parametric study, further study on heat transfer mechanisms, and solar cell performance measurements. For processing capabilities, the ultimate goal is to allow for the system to process an arbitrary area as fast as possible. The increase in speed while maintaining

the annealed spiked structure that has been fabricated through these experiments can come from implementing a scanning mirror instead of the x-y stage. Moving the laser beam instead of the same can be done faster and is more practical for industrial manufacturing processes. At faster speeds, the laser parameters will need to be tuned (i.e. higher pulse power is needed for higher speeds), and the quality of the new structures must be analyzed.

A more extensive parametric study will be carried out. Laser parameters such as beam spot size and wavelength remained constant during this work. Varying these parameters could lead to enhanced structure or processing speeds for the creation of black silicon. Increasing the beam spot size would require more power to get similar results, but would be able to process a given area quicker. The wavelength can be tuned to vary the depth of surface damage, applicable to solar cells with different depths of p-n junctions.

Heat transfer mechanisms will also be further explored. This will be done to see the effect of various mechanisms onto the formation of the microscale structures. These mechanisms include: heating, cooling, phase change, capillary effect, ablation, and plasma shielding.

For characterization, several techniques will be utilized. Carrier lifetime will be measured before and after annealing. Raman spectroscopy will be used to determine the induced stresses and their overall effect on the system. A cross-sectional SEM/FIB analysis will be done to see the height of the textured surface to gain insight on melting depth as well as the aspect ratio of the spikes. Total hemispherical reflectance will be measured by coupling a spectrometer with an integrating sphere. This setup will allow the total absorbance to be calculated. All of the future work presented here is designed to further understand and optimize the creation of black silicon and surface texturing related energy applications.

REFERENCES:

1. Poxson, David J., Mei-Ling Kuo, Frank W. Mont, Y.-S. Kim, Xing Yan, Roger E. Welser, Ashok K. Sood, Jaehee Cho, Shawn-Yu Lin, and E. Fred Schubert. "High-performance antireflection coatings utilizing nanoporous layers." *MRS Bulletin*. 36. (2011): 434-438.
2. Yu, E.T., and J. van de Lagemaat. "Photon management for photovoltaics." MRS BULLETIN. 36. (2011): 424-428.
3. Sher, Meng-Ju, Mark Winkler, and Eric Mazur. "Pulsed-laser hyperdoping and surface texturing for photovoltaics." MRS BULLETIN. 36. (2011): 439-445.
4. Dobrzanski, L.A., A. Drygala, K. Golombek, P. Panek, E. Bielanska, and P. Zieba. "Laser surface treatment of multicrystalline silicon for enhancing optical properties." *Journal of Materials Processing Technology*. (2008): 291-296.
5. Vorobyev, A.Y., and Chunlei Guo. "Direct creation of black silicon using femtosecond laser pulses." *Applied Surface Science*. (2011).
6. Her, Tsing-Hua, Richard J. Finlay, Claudia Wu, Shrenik Deliwala, and Eric Mazur. "Microstructuring of silicon with femtosecond laser pulses." *Applied Physics Letters*. 73. no. 12 (1998): 1673-1675.
7. Zuev, D.A., O.A. Novodvorsky, E.V. Khaydukov, O.D. Khraova, A.A. Lotin, L.S. Parshina, V.V. Rocheva, V.Y. Pachenko, V.V. Dvorkin, A.Y. Poroykov, G.G. Untila, A.B. Chebotareva, T.N. Kost and M.A. Timofeyev. "Fabrication of black multicrystalline silicon surface by nanosecond laser ablation." *Applied Physics B Lasers and Optics*. (2011).
8. California Energy Commission, "Energy Quest." Accessed September 21, 2011. http://www.energyquest.ca.gov/story/chapter08.html.
9. Energy API, "Key Characteristics of Nonrenewable Resources." Last modified August 5, 2008. Accessed September 21, 2011. http://www.api.org/classroom/curricula/nonrenew-resources.cfm.
10. Iudicello, Hiedi. "Alternative Energy Sources." Accessed September 24, 2011. http://www.lhup.edu/smarvel/Seminar/FALL_2004/Iudicello_2/alternative_energy_sources.htm.
11. Folbre, Nancy. "Renewing Support for Renewables." The New York Times, March 28, 2011. http://economix.blogs.nytimes.com/2011/03/28/renewing-support-for-renewables/ (accessed September 24, 2011).
12. U.S. Energy Information Administration, "Renewable & Alternative Fuels." Last modified June 28, 2011. Accessed September 24, 2011. http://www.eia.gov/renewable/annual/preliminary/.
13. Union of Concerned Scientists, "Clean Energy." Last modified December 16, 2009. Accessed September 24, 2011. http://www.ucsusa.org/clean_energy/technology_and_impacts/energy_technologies/how-solar-energy-works.html.
14. Wuerthner, George. "The Truth About Land Use in the United States." Watersheds Messenger. http://www.westernwatersheds.org/watmess/watmess_2002/2002html_summer/article6.htm (accessed September 24, 2011).
15. Green, Martin, Keith Emery, Yoshihiro Hishikawa, Wilhelm Warta, and Ewan Dunlop. "Solar cell efficiency tables (Version 38)." PROGRESS IN PHOTOVOLTAICS: RESEARCH AND APPLICATIONS. (2011): 565-572.
16. AMECO SOLAR, "History of Solar Power." Accessed September 24, 2011. http://www.solarexpert.com/pvbasics2.html.

17. Brighton Webs Ltd., "Statistics for Energy and the Environment." Last modified September 29, 2011. Accessed January 13, 2012. http://www.brighton-webs.co.uk/energy/solar_earth_sun.htm.
18. Bell Labs, "Schawlow and Townes Invent the Laser." Accessed February 3, 2012. http://www.bell-labs.com/history/laser/.
19. Grigoropoulos, Costas P. Transport Laser Microfabrication: Fundamentals and Applications. New York: Cambridge University Press, 2009.
20. Sze, S.M., and Kwok K. Ng. *Physics of Semiconductor Devices: 3rd Edition*. Hoboken: John Wiley & Sons, Inc., 2007.
21. How Stuff Works, "How Lasers Work." Accessed February 26, 2012. http://science.howstuffworks.com/laser3.htm.
22. Amer, M.S., M.A. El-Ashry, L.R. Dosser, K.E. Hix, J.F. Maguire, and Bryan Irwin. "Femtosecond versus nanosecond laser machining: comparison of induced stresses and structural changes in silicon wafers." ELSEVIER. (2004): 162-167.
23. Paschotta, Rudiger, ed. *Encyclopedia of Laser Physics and Technology*. s.v. "Resonator Modes." http://www.rp-photonics.com/resonator_modes.html (accessed March 8, 2012).
24. Hwang, David, and Costas Grigoropoulos. "Efficiency of silicon micromachining by femtosecond laser pulses in ambient air." JOURNAL of APPLIED PHYSICS. 99. (2006).
25. Popa, D., Z. Sun, T. Hasan, F. Torrisi, F. Wang, and A.C. Ferrari. "Graphene Q-switched, tunable fiber laser." *Applied Physics Letters*. 98. no. 7 (2011).
26. Amberg, Gustav, and Minh Do-Quang. "Thermocapillary Convection and Phase Change in Welding." *International Journal of Numerical Methods for Heat & Fluid Flow*. 18. no. 3/4 (2008): 378-386.
27. Coherent, "Lasers in solar Manufacturing." Accessed April 22, 2012.
28. Grohe, Andreas, Annerose Knorz, Jan Nekarda, Ulrich Jager, Nicola Mingirulli, and Ralf Preu. "Novel laser technologies for crystalline silicon solar cell production."
29. Colville, Finlay, and Corey Dunsky. Coherent, "Laser Systems for Photovoltaic Applications." Accessed May 14, 2012.
30. Ostendorf, A., and A. Schoonderbeek. "Lasers in energy device manufacturing."
31. "Lasers Are Making Solar Cells Competitive." *Science Daily*, May 29, 2009.
32. Bartlome, R., B. Strahm, Y. Sinquin, A. Feltrin, and C. Ballif. "Laser application in thin-film photovoltaics." *Applied Physics B Lasers and Optics*. 100. (2010): 427-436.
33. Ocean Optics, "Optical Reflectometer." Accessed April 19, 2012. http://www.directindustry.com/prod/ocean-optics/optical-reflectometers-18485-478195.html.
34. The Physics Classroom, "Specular vs. Diffuse Reflection." Accessed April 19, 2012. http://www.physicsclassroom.com/class/refln/u13l1d.cfm
35. Purdue University, "Scanning ELectron Microscope." Accessed April 19, 2012. http://www.purdue.edu/rem/rs/sem.htm.
36. Fibics Incorporated, "Introduction: Focused Ion Beam Systems." Accessed April 19, 2012. http://www.fibics.com/fib/tutorials/introduction-focused-ion-beam-systems/4/.
37. United Nuclear: Scientific Equipment & Supplies, "Hoffman Apparatus." Accessed April 19, 2012. http://unitednuclear.com/index.php?main_page=product_info&cPath=27_96&products_id=315.
38. Bentor, Yinon. Chemical Elements.com, "Periodic Table: Silicon." Accessed October 17, 2011.
39. "Semiconductor Theory." Accessed October 20, 2011. http://simple- semiconductors.com/.
40. Magcraft, "Conductors, Insulators, and Electron Flow." Accessed October 20, 2011.
41. Electronics-Tutorial, "Semiconductor Basics." Accessed October 23, 2011.

42. Sze, S.M., and Kwok K. Ng. Physics of Semiconductor Devices: 3rd Edition. Hoboken: John Wiley & Sons, Inc., 2007. Pg. 16
43. Maycock, Paul D., and Edward N. Stirewalt. Photovoltaics: Sunlight to Electricity in One Step. Andover: Brick House Publishing Co., 1981.
44. United States Department of Agriculture, "Solar PV (Electric) Energy Self Assessment." Accessed November 12, 2011. http://www.ruralenergy.wisc.edu/renewable/solar_electric/default_solar_electric.aspx.
45. U.S. Department of Energy, "Types of Silicon Used in Photovoltaics." Last modified August 12,2011. Accessed November 13, 2011. http://www.eere.energy.gov/basics/renewable_energy/types_silicon.html
46. U.S. Department of Energy, "Polycrystalline Thin Film Used in Photovoltaics." Last modified August 12,2011. Accessed January 19, 2012. http://www.eere.energy.gov/basics/renewable_energy/polycrystalline_thin_film.html
47. U.S. Department of Energy, "Single-Crystalline Thin Film Used in Photovoltaics." Last modified August 12,2011. Accessed January 19, 2012. http://www.eere.energy.gov/basics/renewable_energy
48. Neuhaus, Dirk-Holger, and Adolf Munzer. "Industrial Silicon Wafer Solar Cells." *Advances in OptoElectronics*. (2007): 1-15
49. "SiOnyx Brings "Black Silicon" into the Light; Material Could Upend Solar, Imaging Industries." *Xconomy*, October 12, 2008
50. Abbott, Malcolm, and Jeffrey Cotter. "Optical and Electrical Properties of Laser Texturing for High-efficiency Solar Cells." *Progress in Photovoltaics: Research and Applications*.
51. Crouch, C.H., J.E. Carey, M. Warrender, M.J. Aziz, and E. Mazur. "Comparison of structure and properties of femtosecond and nanosecond laser-structured silicon." *Applied Physics Letters*. 84. no. 11 (2004): 1850-1852.
52. Kohler , R, H Besser, M Hagen, J Ye, C Ziebert, S Ulrich, J Proell, and W Pfleging. "Laser micro-structuring of magnetron-sputtered SnOx thin films as anode material for lithium on batteries." *Springer*. (2011): 225-232.
53. Garcia-Alonso, D., N Serres, C. Demian, S. Costil, C. Langlade, and C. Coddet. "Pre-/During-/Post0Laser Processes to Enhance the Adhesion and Mechanical Properties of Thermal-Sprayed Coatings with a Reduced Environmental Impact." *Journal of Thermal Spray Technology*. 20. no. 4 (2011): 719-735.
54. Zorba, V., E. Stratakis, M. Barberoglou, E. Spanakis, P. Tzanetakis, and C. Fotakis. "Tailoring the wetting response of silicon surfaces via fs laser structuring." *Applied Physics A*. (2008): 819-825.
55. Cengel, Yunus A. *Heat and Mass Transfer: A Practical Approach*. New York: McGraw-Hill, 2007.
56. Smithsonian Institute, "Fuel Cell Basics." Accessed April 23, 2012. http://americanhistory.si.edu/fuelcells/basics.htm.
57. Ehmann, Kornel. Northwestern University, "Laser-based Texturing." Accessed April 23, 2012.